JNeurosci
THE JOURNAL OF NEUROSCIENCE

Research Articles: Systems/Circuits

Sleep analysis in adult *C. elegans* reveals state-dependent alteration of neural and behavioral responses

https://doi.org/10.1523/JNEUROSCI.1701-20.2020

Cite as: J. Neurosci 2021; 10.1523/JNEUROSCI.1701-20.2020

Received: 2 July 2020
Revised: 18 December 2020
Accepted: 22 December 2020

Sleep analysis in adult *C. elegans* reveals state-dependent alteration of neural and behavioral responses

Authors: Daniel E. Lawler[1], Yee Lian Chew[2], Josh D. Hawk[3], Ahmad Aljobeh[3], William R. Schafer[4], Dirk R. Albrecht[1,5*]

Affiliations:

1. Department of Biomedical Engineering, Worcester Polytechnic Institute, 100 Institute Road, Worcester, MA 01609 USA
2. Illawarra Health and Medical Research Institute and School of Chemistry and Molecular Bioscience, University of Wollongong, Wollongong 2522 Australia
3. Department of Neuroscience, Yale University School of Medicine, P.O. Box 9812, New Haven, CT, 06536-0812, USA
4. Neurobiology Division, Medical Research Council (MRC) Laboratory of Molecular Biology, Francis Crick Avenue, Cambridge CB2 OQH, UK
5. Department of Biology and Biotechnology, Worcester Polytechnic Institute, 100 Institute Road, Worcester, MA 01609 USA

*Correspondence to:

Dirk R. Albrecht, PhD
Department of Biomedical Engineering
Department of Biology and Biotechnology
Worcester Polytechnic Institute
60 Prescott Street, GP4004
Worcester, MA 01605
Phone: 508-831-4859
Email: dalbrecht@wpi.edu

Abbreviated title: Adult *C. elegans* sleep behavior & neural activity

Number of:	pages:	42	Number of words:	abstract:	152
	figures:	9		introduction:	834
	tables:	3			612 w/o refs
	multimedia:	2 movies		discussion:	1378
	3D models:	0			

Acknowledgments

We thank R. Lagoy, K. Burnett, H. White, L. Innarelli, E. Larsen, A. Marley, J. Srinivasan, and D. Colón-Ramos for experimental support and feedback. We thank J. Florman and M. Alkema for graciously providing the AVA::GCaMP imaging line. Some strains were provided by the CGC, which is funded by NIH Office of Research Infrastructure Programs (P40 OD010440). D.R.A. was supported by NSF CBET 1605679 and EF 1724026, NIH R01DC016058, and a Career Award at the Scientific Interface (CASI) from the Burroughs Wellcome Fund. D.E.L. was supported by an NSF IGERT award (DGE 1144804). Y.L.C. was funded by an EMBO Long-term Fellowship (ALTF 403-2016). Research in the D.A.C-R. lab for A.A. and J.D.H. was supported by a Whitman Fellowship from the Marine Biological Laboratories, NIH R01NS076558, DP1NS111778 and by an HHMI Scholar Award. J.D.H. was supported by the Ruth L. Kirschstein NRSA (NIH F32MH105063).

Author contributions

D.E.L. designed and performed experiments, developed methods, analyzed and interpreted data, and wrote the paper. Y.L.C., J.D.H. and W.R.S. interpreted data and developed reagents. A.A. developed reagents. D.R.A. designed experiments, developed methods, analyzed and interpreted data, and wrote the paper.

Conflict of Interest declaration

The authors declare no competing financial interests.

Abstract:

Sleep, a state of quiescence associated with growth and restorative processes, is conserved across species. Invertebrates including the nematode *Caenorhabditis elegans* exhibit sleep-like states during development, satiety and stress. Here we describe behavior and neural activity during sleep and awake states in adult *C. elegans* hermaphrodites using new microfluidic methods. We observed effects of fluid flow, oxygen, feeding, odors, and genetic perturbations on long-term sleep behavior over 12 h. We developed a closed-loop sleep detection system to automatically deliver chemical stimuli to assess sleep-dependent changes to evoked neural responses in individual animals. Sleep increased the arousal threshold to aversive stimulation, yet the associated sensory neuron and first-layer interneuron responses were unchanged. This localizes adult sleep-dependent neuromodulation within interneurons presynaptic to the premotor interneurons, rather than afferent sensory circuits. However, sleep prolonged responses in appetitive chemosensory neurons, suggesting that sleep modulates responsiveness specifically across sensory systems rather than broadly damping global circuit activity.

Significance Statement

Much is known about molecular mechanisms that facilitate sleep control. However, it is unclear how these pathways modulate neural circuit-level sensory processing or how misregulation of neural activity contributes to sleep disorders. The nematode *C. elegans* provides the ability to study neural circuitry with single-neuron resolution, and recent studies examined sleep states between developmental stages and when stressed.

Here, we examine an additional form of spontaneous sleep in adult *C. elegans* at the behavioral and neural activity levels. Using a closed-loop system, we show that delayed behavioral responses to aversive chemical stimulation during sleep arise from sleep-dependent sensorimotor modulation localized presynaptic to the premotor circuit, rather than early sensory circuits.

Introduction

Sleep is a physiological state during which voluntary muscle activity ceases, sensory processing is modulated (Velluti, 1997), and anabolic, growth, and restorative processes occur in the brain and other tissues (Adam and Oswald, 1977). Sleep is observed across species, from mammals to invertebrates (Campbell and Tobler, 1984), where it controls energy usage and metabolism (Schmidt, 2014), macromolecular biosynthesis (Mackiewicz et al., 2007), and neural plasticity and memory consolidation (Frank and Benington, 2006). Owing to these critical functions, sleep deficiencies are associated with impaired cognitive function, productivity (Rajaratnam et al., 2013), and immune response (Luyster et al., 2012) and increased prevalence of cardiovascular disease (Newman et al., 2000), diabetes (Gottlieb et al., 2005), and obesity (Hasler et al., 2004). The initiation and cessation of sleep is mediated in most species by circadian rhythms which are controlled by environmental factors (Reppert and Weaver, 2002) and timing genes that are generally conserved across species (Panda et al., 2002). Several molecular pathways (Kramer et al., 2001; Saper et al., 2005; Sehgal and Mignot, 2011; Siegel, 2004; Tsunematsu et al., 2011; Weber et al., 2015; Yamuy et al., 1999) are involved in promoting sleep states and inhibiting arousal behavior, but it is currently unclear how these pathways modulate neural circuit-level sensory processing during

sleep states (Hennevin et al., 2007), and how misregulation of neural activity may contribute to sleep disorders.

The nematode *C. elegans* provides distinct advantages for direct observation of neurological function in freely-behaving animals. They are small (<1 mm), exhibit short generational times, and have a compact and fully mapped connectome of 302 neurons in hermaphrodites. Noninvasive optical measurements of neural activity can be made in living, behaving animals via genetically-encoded fluorescent calcium indicators such as GCaMP (Tian et al., 2009), and genetic tools are available for rapid generation of mutants and transgenic strains for mechanistic studies (Antoshechkin and Sternberg, 2007; Boulin and Hobert, 2012; Friedland et al., 2013). *C. elegans* demonstrate states of quiescence during lethargus between larval stages (Raizen et al., 2008) ("developmentally-timed sleep") and during periods of stress (Hill et al., 2014), satiety (Gallagher and You, 2014; You et al., 2008), starvation (McCloskey et al., 2017; Skora et al., 2018), and hypoxia (Nichols et al., 2017) ("stress-induced sleep"). Additionally, adult *C. elegans* undergo quiescent periods after 1–2 h of swimming in liquid (Ghosh and Emmons, 2008) and in microfluidic chambers with open and constrictive geometries (Gonzales et al., 2019). Developmentally-timed and stress-induced quiescent states share fundamental sleep functions with other species (Singh et al., 2013), including processing of synaptic plasticity (Dabbish and Raizen, 2011) and metabolic control (Driver et al., 2013). They also share typical behavioral characteristics such as increased arousal threshold (Cho and Sternberg, 2014; Raizen et al., 2008), stereotypical posture (Iwanir et al., 2013; Schwarz et al., 2012; Tramm et al., 2014), homeostatic response to sleep deprivation (Driver et al., 2013; Nagy et al., 2014a;

133 Raizen et al., 2008), and rapid reversibility (Raizen et al., 2008; Trojanowski et al.,
134 2015).
135
136 *C. elegans* sleep has been observed using a variety of experimental platforms, including
137 agar (Raizen et al., 2008) or agarose pads (Churgin et al., 2017; Turek et al., 2015) and
138 microfluidic chambers that house individual animals (Gonzales et al., 2019; Huang et
139 al., 2017; Nagy et al., 2014b; Singh et al., 2011) throughout multiple development
140 stages. Neural activity measurements typically require immobilization by agarose pads
141 (Spies and Bringmann, 2018) or microfluidic traps (Cho and Sternberg, 2014), which
142 limit their use to developmentally-timed or induced sleep studies. However, adult sleep
143 events occur spontaneously and are identified by analysis of locomotion and quiescent
144 behaviors. Thus, in order to assess the functional circuit changes that occur during adult
145 sleep, new methods for monitoring sleep state and stimulated neural responses in
146 freely-moving animals are needed.
147
148 Here we demonstrate two systems to quantify the behavioral and neural characteristics
149 of sleep in young adult *C. elegans*. We first show that sleeping behavior exhibited by
150 young adult *C. elegans* follows characteristic dynamics over 12 h in microfluidic devices
151 and is altered by fluid flow, oxygen, bacterial food, food signals, and genetic
152 perturbations affecting sensory input. Next, using a closed-loop chemical stimulation
153 system, we observed an increased arousal threshold during adult sleep states, as has
154 been observed previously in developmentally-timed sleep (Raizen et al., 2008), and
155 simultaneously monitored neural activity via fluorescence microscopy during these
156 behavioral responses. A sleep-dependent delay in response to aversive stimulation
157 corresponded to diminished and delayed responses in premotor interneurons. However,

158 responses in associated sensory neurons and first-layer interneurons were not
159 modulated by sleep, localizing sleep-state neural circuit modulation within interneurons
160 of the aversive sensorimotor subcircuit. These results suggest that sleep specifically
161 alters the linkage between sensory stimuli and premotor neurons without changing
162 upstream sensory or interneuron information. In contrast, responses in the appetitive
163 sensory neurons were prolonged during sleep, indicating that sleep can affect sensory
164 modalities differently. Together, these results illustrate that sleep modulates neural
165 activity differently across stimuli and validate an experimental system to further dissect
166 the molecular processes that produce this specificity.
167

168 **Materials and Methods**
169

170 **Strains and *C. elegans* culture**

171 All *C. elegans* strains were maintained under standard conditions on NGM plates
172 and fed OP50 *E. coli* bacteria seeded onto each plate. Wild-type animals were Bristol
173 strain (N2). The following mutant strains were used: CB1611, *mec-4 (e1611)*; FK103,
174 *tax-4 (ks28)*; CX32, *odr-10 (ky32)*; IB16, *ceh-17 (np1)*. Neural imaging strains
175 expressing GCaMP in specific neurons were: (AWA (Larsch et al., 2013)) CX14887,
176 *kyIs598* [*gpa-6::GCaMP2.2b*]; (ASH (Larsch et al., 2013)) CX10979, *kyEx2865* [*Psra-*
177 *6::GCaMP3; Pofm-1p::GFP*]; (AIB) DCR6035, *olaIs94* [*Pinx-1::GCaMP6f; Punc-*
178 *122::GFP*]; (AVA) QW607, *zfIs42* [*Prig-3::GCaMP3::SL2::mCherry*] gifted by the Alkema
179 lab; (RIS) AQ4064, *ljEx1119* [*Pflp-11::GCaMP3::SL2-tagRFP;unc-122::rfp*]. To make
180 the RIS imaging line, a 2643 bp region immediately upstream of the ATG of the *flp-11*
181 gene was amplified, similar to previously reported methods (Turek et al., 2016). This
182 promoter was shown to express consistently in RIS and occasionally in other neurons

(Turek et al., 2016). To synchronize for age, we picked L4 larval stage animals one day prior to experimentation such that all animals tested were at the young adult stage.

Animals were transferred to unseeded NGM plates immediately prior to experimentation. The plates were then flooded with the control buffer used for their respective experiment: S. Basal buffer (100 mM NaCl, 50 mM KPO_4; pH 6.0) for unfed behavioral experiments and diacetyl stimulus experiments, S. Medium buffer (1 L S. Basal, 10 mL 1 M potassium citrate pH 6.0, 10 ml trace metals solution, 3 ml 1 M $CaCl_2$, 3 ml 1 M $MgSO_4$) for feeding experiments, or a saline buffer (80 mM NaCl, 5 mM KCl, 20 mM D-glucose, 10 mM HEPES, 5 mM $MgCl_2$, 1 mM $CaCl_2$; pH 7.2) for copper chloride stimulus experiments. Animals were then collected into loading tubing using a 1 mL syringe prior to injection into the microfluidic arena (Lagoy and Albrecht, 2015).

Microfluidic device fabrication

"Population behavior" and "Neural imaging" microfluidic devices were fabricated as previously described (Lagoy and Albrecht, 2015). Briefly, transparency photomasks were printed at 25,000 dpi from designs sketched using DraftSight CAD software. SU-8 mold masters were prepared on silicon wafers using standard photolithography techniques, and microfluidic devices were fabricated by pouring degassed PDMS (Sylgard 184, Dow Corning) onto the mold and heat curing. Individual devices were then cut out and punched to provide inlet and outlet flow. A hydrophobic glass substrate was created by vapor deposition of tridecafluoro-1,1,2,2-tetrahydrooctyl trichlorosilane (TFOCS, Gelest) and then sealed reversibly to the microfluidic channels. An upper glass slide, with holes drilled over inlet and outlet ports with a diamond-coated drill bit, was sealed above the device, which was then was placed into a metal clamp.

Stimulus preparation

All odor dilutions were freshly prepared on the day of experimentation. NA22 *E. coli* stock solutions were prepared using previously described methods (Keil et al., 2017). Briefly, NA22 *E. coli* was cultured, concentrated into pellet form, and suspended in S. medium buffer. A stock solution was diluted to an OD600 of 7.0, and 50 µg/ml of kanamycin was added to prevent bacteria from growing. Chemical solutions were prepared at a 1:20 dilution of stock solution and filtered through a 5 µm filter. Diacetyl (1.1 µM) was prepared from a 10^{-3} dilution (11 mM) stock solution immediately prior to experimentation. Serotonin was prepared by dissolving serotonin creatine sulfate monohydrate powder (Sigma). Sodium sulfite (Sigma) solution was prepared moments before experimentation at 30 mM. We found that a 30 mM sodium sulfite solution would remain at nearly 0% oxygen with stirring for 12 h and without stirring for 5 days (Ocean Optics Neofox O_2 probe kit), so the testing solution would be devoid of oxygen for entire 12 h testing period. The control solution of sodium sulfate was created by allowing for reoxygenation of the sodium sulfite solution for greater than 5 days. For neural imaging experiments, 1 mM copper chloride solution was prepared the day of the experiment using copper chloride powder.

Microfluidic device setup

Microfluidic devices were cleaned, assembled, and degassed in a vacuum desiccator for 30–60 min prior to experimentation. Degassing devices accelerates the absorption of air bubbles within the device. For behavioral experiments, devices were filled with 5% (w/v) Pluronic F127 through the outlet port to prevent bacterial and molecular absorption by passivation of the microfluidic surfaces and to minimize bubble entrapment via its surfactant properties. Neural imaging devices were filled with control

buffer alone. Reservoirs of loading solutions were prepared as previously described (Lagoy and Albrecht, 2015), purging the reservoir system of bubbles and connecting the tubing into the inlets of the device. Once flow was properly established, animals were gently loaded into their respective arenas and allowed to roam for 15–20 min prior to experimentation. For neural imaging experiments, a control valve was used to switch between stimulus and control buffer conditions within 0.5 s (**Fig. 7-1**).

Population behavior imaging and identification of sleep events

Videos of population behavior were captured using a 6.6 MP PixelLink FireWire Camera at 1 fps for 12 h with an image resolution of ~30 pixels/mm. Videos were processed after experimentation as previously described using MATLAB to extract behavioral data (Albrecht and Bargmann, 2011), and then further analyzed to identify sleep events. A minimum sleep entry window of 20 s and exit window of 5 s were used to quantify state transitions. To verify accuracy in parameters for sleep detection, user observed behavioral state was compared to script-calculated state on randomly chosen 60 second traces of an individual animals (**Table 2**). All behavior data was collected using “Population behavior” devices with four 16 mm x 15 mm arenas capable of housing ~25 animals per arena for simultaneous study.

Neural calcium imaging, sleep detection and data analysis in closed-loop system

Closed-loop neural imaging videos were acquired at 5x magnification (NA=0.25) with a Hamamatsu Orca-Flash 4.0 sCMOS camera using MicroManager/ImageJ software. The system has a green (λ = 520-550 nm) LED mounted overhead to provide pulsed brightfield illumination for tracking animal behavior and a Lumencor SOLA-LE solid-state lamp pulsed to excite GCaMP during fluorescence calcium imaging. To

achieve autonomous experimentation for a closed-loop system, custom Arduino, MicroManager, and ImageJ scripts work together to control illumination timing, image acquisition, stimulus delivery, and sleep/wake state identification. An Arduino Uno microcontroller was programmed to control fluidic valves through a ValveLink 8.2 (AutoMate Scientific) controller and to control illumination sources for brightfield and fluorescent imaging. A MicroManager script allows the user to configure all camera and illumination settings prior to experimentation as well as all testing conditions for sleep assessment. Once the experiment is underway, the script initiates brightfield image capture at the desired framerate, and analyzes movement compared with the prior image in real time to determine the animal's behavioral state. If the current state and timing match the desired and preprogrammed conditions for neural imaging, the script initiates a fluorescence image stack recording and communicates with the Arduino via serial commands to control epifluorescence illumination and chemical stimulation with the desired timing.

Tracking of behavior of a single animal in the closed-loop neural imaging system was done using brightfield illumination with images captured at 0.1 fps. The current sleep/awake state of the animal was determined by an ImageJ script which calculates a movement index for each frame, represented as the fraction of body pixels moved since the previous frame, ranging from 0 – 1 (**Fig. 6d**). A sleep state was defined as movement below the empirically-optimized threshold (0.125) for 3 consecutive frames (i.e., for 20–30 s). Optimization of detection parameters was done by maximizing accuracy from user observed behavioral states to script calculated states (**Table 2**). One minute of consistent sleep or wake state frames were used to increase confidence in the animals' current state before neural imaging.

Calcium imaging was performed on freely-moving animals as previously

described (Larsch et al., 2013) using lines expressing GCaMP in selected neurons. Neural activity was recorded in RIS neurons at 2 fps with no stimulation from the closed-loop system, however motion was detected post-processing to identify sleep bouts. Calcium imaging in ASH, AIB, AVA neurons was performed at 10 fps, using closed-loop stimulation to record responses to 10 s chemical stimulation from 5–15 s within a 30 s trial. Calcium imaging in AWA neuron was performed similarly, but was initiated every 5 minutes without closed-loop monitoring; sleep/wake state at stimulus onset was determined post-capture. Videos were analyzed for neural fluorescence and locomotion using NeuroTracker software in ImageJ, which tracks the position of the neuron over time and integrates fluorescent intensity of the soma using a 4 x 4 pixel box for ASH, AIB, and AVA neurons, and an 8 x 8 pixel box for the AWA neuron (Larsch et al., 2013). Fluorescence (F) was normalized by dividing by the initial baseline fluorescence in the first 4 s of each trial before stimulation (F_0). As AIB fluorescence may not be at baseline at the beginning of each trial, baseline AIB intensity was determined for each animal across all trials, and individual AIB traces were excluded when animals engaged in reversal behavior immediately prior to stimulation. Traces and peak data from ASH, AIB, and AVA fluorescence are represented as 1s moving average. Traces and peak data from AWA fluorescence is represented as a 0.3s binned average through the 30 second trials.

The timing of arousal response was defined by the first frame of reversal movement for aversive stimuli, and by the first frame of head movement in sleeping animals stimulated with diacetyl. The onset of neural response was defined as the first frame 3 standard deviations above the pre-stimulation noise level.

Experimental Design and Statistical Analyses

Sample sizes for each experiment are listed in the figure legends. All animals tested were adult hermaphrodites. Statistics were performed using one-way ANOVA with Bonferroni's correction for multiple comparisons or an unpaired two-tailed t-test when specified for 2 sample comparison, using the Statistics and Machine Learning Toolbox in MATLAB. Data are represented as mean ± s.e.m. unless otherwise stated. In behavioral experiments, animals were excluded when valid behavioral tracks comprised <8% of recording time, indicating an animal was not viable or not present during the test. In neural recordings, the top and bottom 1% of instantaneous fluorescent intensity was removed to reduce noise in peak fluorescence calculations. Complete statistical data for all figures reported in **Table 1**.

Software Accessibility

Software for control systems and data analysis are available upon request.

Results

High-throughput analysis of adult sleep

Sleep behavior, defined by periods of behavioral quiescence, was observed in young adult *C. elegans* over 12 hours in microfluidic behavior arenas (Albrecht and Bargmann, 2011). Each microfluidic device contained four 16 mm x 15 mm arenas housing four independent populations of ~25 animals that share the same dynamic, switchable fluidic environment with continuous flow (**Fig. 1a, b**). A hexagonal array of 70 μm tall microposts enables free sinusoidal crawling behavior as animals gain traction from

contact with several microposts along the body (**Fig. 1c**). Wild-type animals roam microfluidic arenas with predominantly forward locomotion, separated by momentary pauses, spontaneous short reversals (<1 s), and long reversals coupled with reorienting "omega" turns (Albrecht and Bargmann, 2011; Gray et al., 2005). Awake animals may pause briefly to feed if bacterial food is present (Flavell et al., 2013) or when encountering obstacles such as other animals or arena barriers. Other times, animals enter a prolonged quiescence state that lasts between ~20 s and several minutes (**Movie 1**). These bouts begin with animals gradually slowing their mean forward locomotion speed over 10–20 s (**Fig. 1d**), often pausing briefly a few times during slow, creeping motion. Animals then gradually adopt a relaxed body posture (Schwarz et al., 2012) over about one minute and cease further movement (**Fig. 1e,f**). Sleeping animals are apparent visually in microfluidic arenas by their straight head and passive contact with only 1 – 2 microposts (**Fig. 1e**), whereas awake animals actively bend around several posts (**Fig. 1c**). After one or more minutes, animals quickly wake and resume forward (or occasionally reverse) locomotion, accelerating to a typical 0.15 mm/s forward velocity within 5 s.

Since pauses reflect both the extended quiescent states of sleep bouts and the momentary pauses of awake animals, true sleep states were automatically identified by tracking centroid movement filtered by the characteristic duration, history, and body shape of sleep. Using temporal parameters based on sleep entry and exit dynamics (onset after 20 s continuous pausing and ending at 5 s non-pausing), automatic classification of sleep bouts showed 95.2% agreement with human observation, with slight underestimation of sleep states (1.9% false discovery rate; 7.9% false omission rate; n = 500 randomly selected bouts; **Table 2**). These detected sleep bouts excluded

the brief pauses that precede a sleep bout, and included momentary “twitch” movements during sleep which can be caused by contact from other animals, flow disturbance, or presumed involuntary movements, and do not signal exit of a sleep state.

We analyzed 535 wild-type (N2) animals for 12 h in continuous slow (0.5 mm/s) flow of S. Basal buffer (**Fig. 2a**). Hourly sleep fraction, defined by the fraction of time the animal spends in a sleep state during each hour, decreased on average across the population from 22% ± 0.8% s.e.m. in the first hour to 8% ± 0.5% in hour 3, then increased steadily to 38% ± 1% in hour 12 (**Fig. 2b**). A wide range of sleep behavior was observed among individual wild-type animals, with 95% exhibiting a 12 h total sleep fraction ranging from 4% to 43%. To assess variability in sleep dynamics, we divided animals into quartiles by total sleep fraction. Sleep dynamics were similar in all quartiles, with sleep fraction increasing over time after 3 h (**Fig. 2b**), but median sleep fraction over 12 h varied greatly across quartiles from 3% to 24%. Median sleep duration remained between 1.3 to 1.9 min for each quartile (**Fig. 2c**), whereas median awake duration varied more greatly, with the top quartile of sleeping animals remaining awake for a median of 7 min, about one-quarter of the most active animals (27 min awake). The increase in sleep fraction from hours 3–12 resulted from longer sleep bouts and shorter awake periods (**Fig. 2d**). These changes were associated with both an increased rate of sleep entry (more sleep pressure) and a decreased rate of sleep exit (more sleepiness) (**Fig. 2e**). The rate of sleep exit remained consistent across total sleep quartiles (**Fig. 2f**), while the rate of sleep entry varied greatly (**Fig. 2g**). Together, these results indicate that individual sleep bouts were similar across wild-type animals, whereas variability in sleep fraction across the population predominantly arose due to variation in frequency of

383 sleep bouts, or equivalently, to variation in the rate of sleep entry and in the duration of
384 awake bouts.
385
386 **Environmental and sensory effects on sleep dynamics**
387
388 Sleep entry and exit are sensitive to environmental conditions and sensory input. To test
389 the role of sensory input on sleep, we first assessed the effect of fluid flow in the
390 microfluidic environment, comparing sleep amounts with a slow flow rate (0.5 mm/s), no
391 flow, and periodic pulsing of flow conditions (**Fig. 3a,b**). Without flow, sleep fraction was
392 similar to moderate flow conditions for the first 3 h, but rose dramatically from 12% to
393 42% around 4 h and remained high (~70%) for the duration of the 12 h experiment (**Fig.**
394 **3a**). To test whether resumption of flow would return sleep fraction to baseline rates, we
395 pulsed flow every 2 h, alternating between 0.5 mm/s flow or no flow. Again, sleep
396 fraction remained low for the first 3 h regardless of flow condition, then increased during
397 each flow stoppage after about 30 mins and decreased sharply when flow resumed
398 (**Fig. 3b**).
399
400 Sleep fraction when flow resumed fell below measurements in continuous flow,
401 suggesting evidence of a homeostatic sleep mechanism, in which periods of elevated
402 sleep are followed by reduced sleep, and vice versa. We tested this further by
403 subjecting animals to a no flow condition for 6 hours, during which they slept more
404 (+26.8% ± 9.5%, P=0.03, t-test) than control animals in continuous flow after 2 hours of
405 acclimation (**Fig. 3c**). Upon resumption of flow, these animals then slept significantly
406 less (-14.3% ± 5.8%, $P=8.13\times10^{-5}$, t-test) than control animals over the following 6
407 hours. Conversely, reducing sleep with 1.1 μM diacetyl (-7.4% ± 1.8%, P=0.031, t-test)

resulted in a compensatory increase (+11.5% ± 4.7%, $P=1.84x10^{-5}$, t-test) in sleep fraction compared with controls that persisted for several hours (**Fig. 3d**). Together, these results demonstrate a bidirectional homeostatic sleep response.

Under static conditions, animals can deplete the microfluidic environment of oxygen (Huang and Lin, 2018; Suda et al., 2005), and hypoxia has been shown to induce sleep behavior (Kim and Jin, 2015) especially in starved animals (Skora et al., 2018). We therefore assessed the role of oxygen in adult sleep in microfluidic devices. With continuous flow of 0.5 mm/s, a hypoxic buffer (<1% O_2, 30 mM sodium sulfite (Jiang et al., 2011)) significantly increased total sleep fraction over 12 h (48% ± 1.1%, $P=1.74x10^{-43}$, ANOVA) compared to the same solution reoxygenated to >20% O_2 (16% ± 1.3%) (**Fig. 4a-c**). During hypoxia, 13% of sleep bouts were >10 min long compared to only 3.5% of bouts in the reoxygenated buffer, and 1% of hypoxic sleep bouts lasted over 30 mins (**Fig. 4b**). Notably, hypoxia increased sleep fraction only after 4 h in the device (**Fig. 4c**), in line with past results suggesting that starvation and hypoxia work together to promote sleep behavior (Skora et al., 2018). The rapid rise in sleep behavior after 4 h mimicked a similar rise in static no-flow conditions (**Fig. 3a**), suggesting that gentle flow replenishes oxygen to suppress sleep behavior.

Because feeding state impacts arousal (Chao et al., 2004; Ezcurra et al., 2016) and starvation may regulate the impact of hypoxia on sleep (Skora et al., 2018), we next assessed the role of feeding and satiety on adult sleep dynamics within microfluidic chambers (**Fig. 4d-f**). The presence of bacterial food (NA22 *E. coli*) suppressed total 12 h average sleep fraction (3.8% ± 0.6%, $P=2.83x10^{-123}$, ANOVA) compared to S. Basal control (33% ± 0.5%) (**Fig. 4e**). Serotonin, which mimics the feeding response (Horvitz

et al., 1982), similarly reduced total sleep fraction (8% ± 1.1%, $P=4.21x10^{-103}$, ANOVA) compared to control buffer conditions when presented at a moderate concentration of 10 μM. Whereas bacterial food suppressed sleep continuously for 12 h, serotonin suppressed sleep for the first ~9 h. Similarly, a moderate behaviorally attractive food odor (Chuang and Collins, 1968) (1.1 μM diacetyl) suppressed total sleep fraction compared to control buffer (28% ± 0.9%, $P=3.13x10^{-8}$, ANOVA), although to a lesser extent than food or serotonin. Diacetyl suppressed sleep fraction only up to hour 9, consistent with adaptation to the odor over hours (Larsch et al., 2015; Matsuura et al., 2009) (**Fig. 4f**). Animals also slept more when starved longer on a plate without food prior to entry into the microfluidic environment (**Fig. 4g,h**). These results suggest that adult sleep behavior in microfluidic devices is driven in part by feeding state and the perception of hunger.

To observe how sensory information influences sleep, we tested wild-type animals and three sensory mutants (**Fig. 5a-c**) loaded into separate arenas of each "Population behavior" device (**Fig. 1a**). Since the odorant diacetyl reduced sleep (**Fig. 4f**), we tested *odr-10* mutants, which lack the diacetyl receptor normally present in the AWA sensory neurons and should not perceive this odor. In the presence of 1.1 μM diacetyl, *odr-10* mutants exhibited a higher total sleep fraction (40% ± 1.0%, $P=2.93x10^{-11}$, ANOVA) compared to wild-type (28% ± 1.2%) (**Fig. 5b**), and similar to wild-type animals in control buffer conditions lacking the odor (**Fig. 5-1**). In diacetyl, *odr-10* mutants showed a significant increase in hourly sleep fraction compared to wild-type only up to 8 h (**Fig. 5c**), after which habituation to the odor may reduce its influence. Sensory deficient *tax-4* mutants lack a cyclic GMP-gated ion channel necessary for signal transduction in many sensory neurons (Komatsu et al., 1996) and are defective in multiple sensory behaviors,

458 failing to respond to temperature or to water-soluble or volatile chemical cues. However,
459 *tax-4* is not present in AWA neurons; hence, diacetyl-mediated sleep suppression
460 should be preserved in this mutant. Indeed, while *tax-4* showed a moderate decrease in
461 total sleep fraction (20.7% ± 1.0%, $P=2.66\times10^{-5}$, ANOVA) compared to wild-type over 12
462 h in 1.1 µM diacetyl, no significant differences in hourly sleep fraction were observed
463 except during the first hour (**Fig. 5c**). Strong suppression of early quiescence bouts in
464 hour 1 in *tax-4* animals (4% vs. 21%) suggests that sensory information other than from
465 AWA neurons contributes to elevated quiescence in the first hour. Animals transferred
466 into microfluidic devices experience a novel mechanical environment, including gentle
467 touch of the microposts and continuous fluid flow. While gentle touch deficient *mec-4*
468 mutants showed a slightly lower total sleep fraction than wild-type (24% ± 1.0% vs. 28%
469 ± 1.2%, P=0.005, ANOVA), *mec-4* mutants had no significant difference in first hour
470 sleep fraction compared with wild-type (18% vs. 21%), suggesting that any sensory
471 information leading to elevated initial quiescence did not come from the *mec-4*-
472 expressing touch receptor neurons ALM, AVM, or PLM. Together, these data
473 demonstrate the role of sensory information in sleep regulation, and the testing of
474 multiple mutants at once in multi-arena microfluidic devices to investigate regulators of
475 sleep dynamics.
476
477 Stress-induced sleep is altered in *ceh-17* mutants, in which the ALA neurons fail to
478 develop normally (Pujol et al., 2000). These animals are resistant to *lin-3*/EGF-induced
479 sleep (Buskirk and Sternberg, 2010) and exhibit lower levels of quiescence after
480 exposure to stressors such as heat shock, hyperosmosis, alcohol, cold, and toxins (Hill
481 et al., 2014). However, spontaneous adult sleep in *ceh-17* mutants was significantly
482 higher over 12 h (43% ± 0.9%, $P=1.47\times10^{-23}$, ANOVA) compared to wild-type (26.5% ±

0.9%) animals in unrestrained microfluidic arenas (**Fig. 5d-f**), suggesting that it differs from ALA-dependent stress-induced sleep.

Automatic sleep tracking, chemical stimulation, and neural imaging

To understand how neural activity changes during sleep cycles, we designed a smaller "Neural imaging" microfluidic device containing a single 3 mm x 3 mm arena with the same micropost array as the "Population behavior" device (**Fig. 6a**), but sized to fit the entire field of view at 5x magnification on an epifluorescence microscope (**Fig. 6b**). Wild-type *C. elegans* sleep dynamics in the small "Neural imaging" device were equivalent to the larger "Population behavior" devices, dropping from 18% to 6% over the first 3 h, then steadily rising to 50% by 12 h, despite a faster flow velocity in the neural imaging microfluidic device (15 mm/s vs. 0.5 mm/s) (**Fig. 6c**). Sleep behavior was tracked using brightfield illumination every 10 s, using a frame subtraction algorithm similar to previous methods (Nagy et al., 2014b) (**Fig. 6d,e**), and correctly identified sleep bouts with 93.4% agreement with human observers (**Table 3**).

The "Neural imaging" device provides fast temporal control of chemical stimuli, capable of reproducible fluid switching in <0.5 s (**Fig. 7-1**) without disturbing natural behaviors. We assessed arousal threshold by testing sensory responsiveness of sleeping and awake wild-type animals to aversive 10-s pulses of 1 mM copper chloride solution, recording the time elapsed between chemical onset and the initial reversal movement response. Sleep or wake states were determined by average pixel movement 5 s prior to stimulation (**Fig. 7a**), which was significantly higher in awake vs. sleeping states (58.1 ± 15.3 μm/s vs. 3.2 ± 0.7 μm/s, $P=3.2\times10^{-4}$, t-test) (**Fig. 7b**). Reversal responses in a

508 sleep state were about eight times slower (6.0 s ± 1.2 s, P=0.0014, t-test) than in an
509 awake state (0.76 s ± 0.14 s). This delay is consistent with an increased threshold for
510 sensory responsiveness in sleeping young adult animals (**Fig. 7c**), as has been shown
511 during lethargus to mechanical and chemical stimuli in developmentally-timed sleep
512 (Raizen et al., 2008).
513
514 RIS interneuron activity correlates with the onset of developmentally-timed sleep
515 (Maluck et al., 2020; Turek et al., 2013) and quiescent behavior in adults (Steuer Costa
516 et al., 2019). To demonstrate neural imaging during spontaneous sleep-wake cycles in
517 the microfluidic device, we recorded activity in the RIS interneuron expressing GCaMP3
518 (**Fig. 7d**) in freely moving animals while simultaneously assessing movement behavior.
519 As expected, RIS activity increased at the onset of adult sleep (**Fig. 7e**).
520
521 **Closed-loop stimulation and neural imaging of a reversal circuit**
522
523 An increased threshold for sensory responsiveness during sleep suggests sleep-
524 dependent modulation to neural activity in *C. elegans*, either in sensory responses to
525 stimulation, or in downstream interneurons or motor neurons. For example, during
526 lethargus states in developmentally-timed sleep, aversive chemical pulses (1 mM
527 copper chloride) elicited weaker ASH sensory neuron activity (Cho and Sternberg,
528 2014). However, it is unclear whether sensory-level modulation occurs during adult
529 sleep as well. Since adult sleep is not synchronized across animals, or within an
530 individual, we developed a closed-loop system that monitors sleep state every 10 s and
531 triggers a stimulation and neural recording when user-programmable conditions are met
532 (**Fig. 8a, Movie 2**). Here, we chose to stimulate one minute after a sleep state

transition, allowing a 15-minute recovery period between stimulation trials (**Fig. 8b**). Brief pulses of blue light excitation were used for fluorescent imaging to measure calcium activity during each 30-s trial (**Fig. 8c**), as strong blue light can cause arousal by itself (Edwards et al., 2008), and sleep state was monitored by behaviorally-neutral green light.

We measured neural responses to 10-s pulses of 1 mM copper chloride in the ASH sensory neurons over 12 h in individual animals. A typical closed-loop experiment with 15-minute recovery per stimulation recorded about one sleep and one awake response per hour over >10 hours (**Fig. 8d,e, Fig. 8-1**). ASH neurons responded strongly and consistently to each copper chloride pulse, regardless of sleep or awake state during stimulation (**Fig. 8f,g**), and showed no significant sensory adaptation (**Fig. 8e**).

Since ASH chemosensory responses were equivalent in sleep and awake states, the elevated arousal threshold in sleep could result from diminished activity in interneurons, motor neurons, or in the muscles themselves. ASH is directly presynaptic to AVA premotor interneurons, and also has secondary connections through AIB, AVD, and RIC interneurons (**Fig. 8-2**). As AIB shares a gap junction with the sleep-inducing neuron RIS, and ablation of AIB reduces long reversals (Gray et al., 2005), we recorded AIB and AVA neural activity in sleep and awake states in response to 1 mM copper chloride. Neural responses in AIB were not significantly different between awake and sleep states (**Fig. 8h,i**). In contrast, animals in sleep states had diminished AVA responses, increasing average relative GCaMP fluorescence 48% when awake and 19% when asleep (P=0.031, t-test). AVA neural responses were also delayed relative to the copper pulse (**Fig. 8j,k**), consistent with delayed and shortened reversal behaviors (**Fig. 7c**).

AIB activity often increased before reversal behavior in sleeping animals but coincided with reversal responses in awake animals (**Fig. 8-3**). This suggests a sleep-dependent behavioral delay downstream of (or bypassing) AIB and presynaptic to AVA, that contributes to the apparent arousal threshold increase in sleeping animals.

Appetitive sensory modulation during sleep

Sleep may affect sensory modalities differently. To compare with ASH aversive response circuits, we assessed sleep-dependent changes in an appetitive sensory circuit using the AWA chemosensory neurons. Whereas aversive stimulation of ASH with copper chloride provoked reversal behavior in both sleeping and awake animals, appetitive stimulation of AWA with 1.1 μM diacetyl elicited slight head movement in sleeping animals and promoted a continuation of forward locomotion behavior in awake animals (**Fig. 9a**). Since awake animals experienced no strong behavior change upon presentation of appetitive stimuli, sleep-dependent arousal timing differences could not be made. However, simultaneous measurements of neural activity revealed sleep-dependent differences in neural response (**Fig. 9b**).

Animals that were sleeping prior to diacetyl stimulation responded with a ~2 s delay in initial movement (3.25 ± 0.15 s after stimulation onset, $P=2.11\times10^{-13}$, t-test) compared to the initial rise in AWA activity (1.21 ± 0.05 s after stimulation onset; **Fig. 9c**). This sleep-dependent response delay was shorter and more consistent than with copper chloride stimulation. AWA neural activity arose equally in awake and sleeping animals at stimulus onset (**Fig. 9b,d**), but AWA activity remained high throughout the 10-s diacetyl pulse in sleeping animals, whereas it declined about 5 s earlier in awake animals (**Fig.**

583 **9d**). As a result, AWA neural responses were significantly elevated during the 15 s after
584 stimulation in sleeping animals (0.54 ± 0.04 dF/F_0, $P=1.18x10^{-5}$, t-test) than awake
585 animals (0.19 ± 0.05 dF/F_0; **Fig. 9e**). While sleep prolonged sensory neural dynamics in
586 AWA to 1.1 μM diacetyl, peak response levels were unchanged across sleep and
587 awake states, as were ASH responses to 1 mM copper chloride (**Fig. 9f**).
588
589 **Discussion**
590
591 *C. elegans* sleep has been studied previously during developmentally-timed transitions
592 (lethargus) and after induction by satiety or various stresses, but spontaneous adult
593 sleep has been technically more difficult to assess. Adult quiescence behavior in our
594 microfluidic arena devices displays the same general characteristics of sleep previously
595 used to define quiescent behavior as sleep in *C. elegans* during developmentally-timed
596 sleep and stress-induced sleep. Quiescent adults exhibited: (1) an increase in arousal
597 threshold to an aversive chemical stimulus by a delay in behavioral response (**Fig. 7c**),
598 (2) rapid sleep reversibility upon changes in fluid flow (**Fig. 3b**), (3) a characteristic
599 relaxed posture (**Fig. 1e,f**), and (4) a homeostatic sleep response (**Fig. 3c,d**). We
600 observed some differences in unrestrained adult sleep behavior compared with recent
601 reports on adult sleep in open and constrained environments, which we attribute to
602 microfluidic geometry and experiment duration. For example, static fluids and hypoxia
603 were highly somnolent in freely-behaving animals over 12 h, whereas constricted
604 animals increased sleep during gentle microfluidic flow, with no effect of oxygen over 1
605 h (Gonzales et al., 2019). Spontaneous adult sleep was elevated in *ceh-17* mutant
606 animals, which are deficient in stress-induced sleep, suggesting that spontaneous adult

607 sleep in unrestrictive microfluidic devices is unique to the sleep states previously
608 observed.
609
610 Sleep and hunger are mutually inhibitory. In mammals, the hunger-associated peptide
611 ghrelin suppresses sleep, whereas satiety-related leptin and insulin promote sleep
612 (Goldstein et al., 2018). In *C. elegans*, adult sleep behavior was also strongly
613 suppressed by continuous food presentation for the entire 12 h experiment duration. In
614 contrast, well-fed animals introduced into buffer without food gradually increased their
615 sleep fraction over several hours, and pre-starvation commensurately accelerated this
616 timing. Presenting exogenous serotonin to mimic the feeding response, or the food odor
617 diacetyl, suppressed sleep for 8 – 9 h, consistent with adaptation timing to these food-
618 related signals.
619
620 Sleep behavior is also sensitive to environmental conditions presented in microfluidic
621 devices. For example, fluid flow in the microfluidic environment is important for
622 maintaining a fresh and constant environment, and cessation of flow increased sleep
623 behavior dramatically after several hours. Static fluid conditions decrease mechanical
624 stimulation, deplete nutrients and oxygen, and increase concentrations of byproducts
625 and CO_2. Oxygen depletion by animals may be a primary factor driving elevated sleep
626 in static microfluidic conditions, as sleep dynamics were similar in static fluid and with
627 hypoxic buffer flow. Hypoxia increased sleep behavior only after 4 h in freely-behaving
628 animals, likely due to increasing starvation over this time. Similarly, hypoxia was shown
629 to suppress most spontaneous neural activity across the whole brain of trapped *C.*
630 *elegans,* but only in starved animals (Skora et al., 2018). In mammals, intermittent
631 hypoxia can cause excessive sleepiness (Sanfilippo-Cohn et al., 2006), but can also

632 cause disturbed and superficial sleep with frequent waking via chemoreceptor reflex
633 pathways (Laszy and Sarkadi, 1990). Thus, there is an interplay between arousing and
634 somnolent environmental cues, in addition to feeding state. Further studies in *C.*
635 *elegans* may be useful to distinguish between these contrasting hypoxic effects and to
636 understand the role of sleep in regulating metabolic systems.
637
638 Sensory neural activity directly modulates sleep. For example, sleep suppression by
639 diacetyl was absent in *odr-10* mutants that lack only the diacetyl receptor and are
640 unable to detect this odor. Sensory information and fluid flow also contribute to the initial
641 elevated sleep behavior seen in the first hour of testing as animals acclimate to the
642 microfluidic environment. The general sensory mutant *tax-4* suppressed first-hour sleep
643 whereas mechanosensory-deficient *mec-4* animals did not, suggesting that gentle touch
644 of microfluidic structures do not contribute to early sleep behavior. Instead, other *tax-4*
645 dependent sensation, such as from various thermo- and chemosensory neurons
646 (Komatsu et al., 1996), may be involved in detecting the novel microfluidic environment.
647
648 We compared activity of several neurons during sleep and awake states of unrestrained
649 animals. The RIS interneuron is active at the onset of spontaneous adult sleep, as has
650 been shown during developmentally-timed lethargus sleep (Maluck et al., 2020; Turek
651 et al., 2013). The automated closed-loop stimulation system, which requires no user
652 input, further allows unbiased comparison of stimulus-evoked neural responses during
653 alternating sleep and awake bouts within the same animal. The ability to record state-
654 dependent response differences within individuals is particularly important due to the
655 wide variation in sleep dynamics observed across individual animals. Isogenetic
656 animals, even when raised on the same plate from the same parent, exhibited total

657 sleep fractions varying from zero to nearly one half over 12 h. Given the sensitivity of
658 adult sleep to oxygen, feeding state, chemicals, and likely other sensory stimuli, it is
659 possible that animals cultured identically experience slight variations in these inputs.
660 Longitudinal studies capturing dozens of events per animal allow identification of intra-
661 animal differences in sensory processing irrespective of population-wide variation in
662 sleep patterns.
663
664 An increased arousal threshold in sleeping animals suggests modulation to
665 sensorimotor neural circuit activity in *C. elegans* during sleep. Responses of the AVA
666 command interneurons, which are required for backward locomotion (Gray et al., 2005;
667 Piggott et al., 2011; Zheng et al., 1999) were indeed diminished and delayed during
668 adult sleep, coinciding with delayed behavioral responses. Similarly, diminished AVA
669 activity was previously observed during lethargus (Cho and Sternberg, 2014). However,
670 sensory responses in ASH neurons were not modulated by sleep state in adults, in
671 contrast to the weaker ASH responses observed in larval stages during
672 developmentally-timed sleep (Cho and Sternberg, 2014), suggesting that spontaneous
673 adult sleep is a distinct phenomenon. The first layer AIB interneurons, which share
674 synaptic connections with ASH, the AVA command interneurons, and the RIS sleep-
675 induction neuron, also showed no sleep-dependent difference in response. Together,
676 these results suggest that modulation in sensory processing that leads to reduced
677 arousal response in sleep occurs at or upstream of AVA, such as synaptic signaling
678 from ASH, AIB, or other interneurons (**Fig. 8-2**), or neuropeptides from other sources.
679 One possibility is that sleep increases arousal threshold predominately by diminishing
680 the efficacy of monosynaptic shortcuts to the command interneurons (here, ASH to
681 AVA), whereas sensory information is preserved to first layer interneurons (such as AIB)

682 to allow for rapid arousal from more salient polymodal stimuli from multiple sensory
683 neurons. However, animal survival should benefit from maintaining rapid arousal to
684 potentially harmful stimuli such as sensed by ASH, yet this does not appear true.
685 Alternatively, the dampened brain state apparent in sleep (Nichols et al., 2017) may
686 broadly suppress activity in premotor interneurons like AVA, increasing arousal
687 thresholds equally to all types of sensory input which result in reversal behavior.
688
689 But sleep influences sensory modalities differently. The appetitive stimulus diacetyl
690 aroused sleeping animals after several seconds, just as the aversive stimulus, although
691 the stimulus-to-behavior delay was shorter and more consistent (2.5 – 4.4 s to
692 appetitive forward response vs. 1 – 14 s to aversive reversal response). Further, AWA
693 sensory responses to diacetyl were prolonged in the sleep state, unlike ASH aversive
694 responses. While locomotory feedback is processed by sensorimotor circuits (Hendricks
695 et al., 2012), past studies have shown no AWA response differences between crawling
696 and paralyzed animals (Larsch et al., 2013). This suggests that differences seen in
697 neural response in AWA are due to sleep related mechanisms rather than feedback
698 from locomotion alone. Together, these differences suggest that sleep-dependent circuit
699 modulation acts differently across sensory circuits, and further study of additional
700 sensory stimuli and neurons will be necessary to uncover its architecture and
701 mechanisms.
702
703 These flexible microfluidic systems for studying adult sleep in *C. elegans* are applicable
704 to any neuron, stimulus, environment, and genetic perturbation for thorough
705 assessment of sleep behavior and underlying neural responses. For example, it will be
706 informative to compare neural responses in various sleep modes, including hypoxia and

starvation-induced sleep as shown here, as well as heat shock and satiety-related sleep. Microfluidic devices are easily customized to different animal sizes by adjusting arena post geometry, for example, to observe L4 animals in lethargus transition stages in developmentally-timed sleep. Other types of oxidative or metabolic stress (such as by chemical oxidants or varying food quality), or sleep disruption via mechanical stimulation or light, can be applied using the same microfluidic devices and tracking methods. Overall, this platform can be used to uncover molecular and neural circuit pathways underlying altered sensation during sleep, toward establishing connections between nematode sleep and associated regulatory mechanisms and human sleep disorders.

References

Adam, K., and Oswald, I. (1977). Sleep Is for Tissue Restoration. J R Coll Physicians Lond *11*, 376–388.

Albrecht, D.R., and Bargmann, C.I. (2011). High-content behavioral analysis of Caenorhabditis elegans in precise spatiotemporal chemical environments. Nat Meth *8*, 599–605.

Antoshechkin, I., and Sternberg, P.W. (2007). The versatile worm: genetic and genomic resources for Caenorhabditis elegans research. Nat Rev Genet *8*, 518–532.

Boulin, T., and Hobert, O. (2012). From Genes to Function : The C. elegans Genetic Toolbox. Wiley Interdiscip Rev Dev Biol *1*, 114–137.

Buskirk, C.V., and Sternberg, P.W. (2010). Paired and LIM class homeodomain proteins coordinate differentiation of the C. elegans ALA neuron. Development *137*, 2065–2074.

Campbell, S.S., and Tobler, I. (1984). Animal sleep: A review of sleep duration across phylogeny. Neuroscience & Biobehavioral Reviews *8*, 269–300.

Chao, M.Y., Komatsu, H., Fukuto, H.S., Dionne, H.M., and Hart, A.C. (2004). Feeding status and serotonin rapidly and reversibly modulate a Caenorhabditis elegans chemosensory circuit. PNAS *101*, 15512–15517.

Cho, J.Y., and Sternberg, P.W. (2014). Multilevel Modulation of a Sensory Motor Circuit during C. elegans Sleep and Arousal. Cell *156*, 249–260.

Chuang, L.F., and Collins, E.B. (1968). Biosynthesis of Diacetyl in Bacteria and Yeast. J Bacteriol *95*, 2083–2089.

Churgin, M.A., Jung, S.-K., Yu, C.-C., Chen, X., Raizen, D.M., and Fang-Yen, C. (2017). Longitudinal imaging of Caenorhabditis elegans in a microfabricated device reveals variation in behavioral decline during aging. Elife *6*.

Dabbish, N.S., and Raizen, D.M. (2011). GABAergic Synaptic Plasticity during a Developmentally Regulated Sleep-Like State in C. elegans. J. Neurosci. *31*, 15932–15943.

Driver, R.J., Lamb, A.L., Wyner, A.J., and Raizen, D.M. (2013). DAF-16/FOXO Regulates Homeostasis of Essential Sleep-like Behavior during Larval Transitions in C. elegans. Current Biology *23*, 501–506.

Edwards, S.L., Charlie, N.K., Milfort, M.C., Brown, B.S., Gravlin, C.N., Knecht, J.E., and Miller, K.G. (2008). A Novel Molecular Solution for Ultraviolet Light Detection in Caenorhabditis elegans. PLoS Biol *6*, e198.

Ezcurra, M., Walker, D.S., Beets, I., Swoboda, P., and Schafer, W.R. (2016). Neuropeptidergic Signaling and Active Feeding State Inhibit Nociception in Caenorhabditis elegans. J Neurosci *36*, 3157–3169.

754 Flavell, S.W., Pokala, N., Macosko, E.Z., Albrecht, D.R., Larsch, J., and Bargmann, C.I.
755 (2013). Serotonin and the Neuropeptide PDF Initiate and Extend Opposing Behavioral
756 States in C. elegans. Cell *154*, 1023–1035.

757 Frank, M.G., and Benington, J.H. (2006). The Role of Sleep in Memory Consolidation
758 and Brain Plasticity: Dream or Reality? Neuroscientist *12*, 477–488.

759 Friedland, A.E., Tzur, Y.B., Esvelt, K.M., Colaiácovo, M.P., Church, G.M., and Calarco,
760 J.A. (2013). Heritable genome editing in *C. elegans* via a CRISPR-Cas9 system. Nature
761 Methods *10*, 741–743.

762 Gallagher, T., and You, Y.-J. (2014). Falling asleep after a big meal: Neuronal
763 regulation of satiety. Worm *3*, e27938.

764 Ghosh, R., and Emmons, S.W. (2008). Episodic swimming behavior in the nematode C.
765 elegans. Journal of Experimental Biology *211*, 3703–3711.

766 Goldstein, N., Levine, B.J., Loy, K.A., Duke, W.L., Meyerson, O.S., Jamnik, A.A., and
767 Carter, M.E. (2018). Hypothalamic Neurons that Regulate Feeding Can Influence
768 Sleep/Wake States Based on Homeostatic Need. Current Biology *28*, 3736-3747.e3.

769 Gonzales, D.L., Zhou, J., Fan, B., and Robinson, J.T. (2019). A microfluidic-induced C.
770 elegans sleep state. Nature Communications *10*, 1–13.

771 Gottlieb, D.J., Punjabi, N.M., Newman, A.B., Resnick, H.E., Redline, S., Baldwin, C.M.,
772 and Nieto, F.J. (2005). Association of sleep time with diabetes mellitus and impaired
773 glucose tolerance. Arch. Intern. Med. *165*, 863–867.

774 Gray, J.M., Hill, J.J., and Bargmann, C.I. (2005). A circuit for navigation in
775 Caenorhabditis elegans. Proc. Natl. Acad. Sci. U.S.A. *102*, 3184–3191.

776 Hasler, G., Buysse, D.J., Klaghofer, R., Gamma, A., Ajdacic, V., Eich, D., Rössler, W.,
777 and Angst, J. (2004). The association between short sleep duration and obesity in
778 young adults: a 13-year prospective study. Sleep *27*, 661–666.

779 Hendricks, M., Ha, H., Maffey, N., and Zhang, Y. (2012). Compartmentalized calcium
780 dynamics in a C. elegans interneuron encode head movement. Nature *487*, 99–103.

781 Hennevin, E., Huetz, C., and Edeline, J.-M. (2007). Neural representations during sleep:
782 From sensory processing to memory traces. Neurobiology of Learning and Memory *87*,
783 416–440.

784 Hill, A.J., Mansfield, R., Lopez, J.M.N.G., Raizen, D.M., and Van Buskirk, C. (2014).
785 Cellular Stress Induces a Protective Sleep-like State in C. elegans. Current Biology *24*,
786 2399–2405.

787 Horvitz, H.R., Chalfie, M., Trent, C., Sulston, J.E., and Evans, P.D. (1982). Serotonin
788 and Octopamine in the Nematode Caenorhabditis elegans. Science *216*, 1012–1014.

789 Huang, S.-H., and Lin, Y.-W. (2018). Bioenergetic Health Assessment of a Single
790 Caenorhabditis elegans from Postembryonic Development to Aging Stages via

791 Monitoring Changes in the Oxygen Consumption Rate within a Microfluidic Device.
792 Sensors (Basel) *18*.

793 Huang, H., Singh, K., and Hart, A.C. (2017). Measuring Caenorhabditis elegans Sleep
794 During the Transition to Adulthood Using a Microfluidics-based System. Bio Protoc *7*.

795 Iwanir, S., Tramm, N., Nagy, S., Wright, C., Ish, D., and Biron, D. (2013). The
796 Microarchitecture of C. elegans Behavior during Lethargus: Homeostatic Bout
797 Dynamics, a Typical Body Posture, and Regulation by a Central Neuron. Sleep *36*,
798 385–395.

799 Jiang, B., Ren, C., Li, Y., Lu, Y., Li, W., Wu, Y., Gao, Y., Ratcliffe, P.J., Liu, H., and
800 Zhang, C. (2011). Sodium sulfite is a potential hypoxia inducer that mimics hypoxic
801 stress in Caenorhabditis elegans. J Biol Inorg Chem *16*, 267–274.

802 Keil, W., Kutscher, L.M., Shaham, S., and Siggia, E.D. (2017). Long-term high-
803 resolution imaging of developing C. elegans larvae with microfluidics. Dev Cell *40*, 202–
804 214.

805 Kim, K.W., and Jin, Y. (2015). Neuronal responses to stress and injury in C. elegans.
806 FEBS Lett *589*, 1644–1652.

807 Komatsu, H., Mori, I., Rhee, J.-S., Akaike, N., and Ohshima, Y. (1996). Mutations in a
808 Cyclic Nucleotide–Gated Channel Lead to Abnormal Thermosensation and
809 Chemosensation in C. elegans. Neuron *17*, 707–718.

810 Kramer, A., Yang, F.-C., Snodgrass, P., Li, X., Scammell, T.E., Davis, F.C., and Weitz,
811 C.J. (2001). Regulation of Daily Locomotor Activity and Sleep by Hypothalamic EGF
812 Receptor Signaling. Science *294*, 2511–2515.

813 Lagoy, R.C., and Albrecht, D.R. (2015). Microfluidic Devices for Behavioral Analysis,
814 Microscopy, and Neuronal Imaging in Caenorhabditis elegans. In C. Elegans, D. Biron,
815 and G. Haspel, eds. (Humana Press), pp. 159–179.

816 Larsch, J., Ventimiglia, D., Bargmann, C.I., and Albrecht, D.R. (2013). High-throughput
817 imaging of neuronal activity in Caenorhabditis elegans. PNAS *110*, E4266–E4273.

818 Larsch, J., Flavell, S.W., Liu, Q., Gordus, A., Albrecht, D.R., and Bargmann, C.I. (2015).
819 A Circuit for Gradient Climbing in C. elegans Chemotaxis. Cell Rep *12*, 1748–1760.

820 Laszy, J., and Sarkadi, A. (1990). Hypoxia-induced sleep disturbance in rats. Sleep *13*,
821 205–217.

822 Luyster, F.S., Strollo, P.J., Zee, P.C., and Walsh, J.K. (2012). Sleep: A Health
823 Imperative. Sleep *35*, 727–734.

824 Mackiewicz, M., Shockley, K.R., Romer, M.A., Galante, R.J., Zimmerman, J.E., Naidoo,
825 N., Baldwin, D.A., Jensen, S.T., Churchill, G.A., and Pack, A.I. (2007). Macromolecule
826 biosynthesis: a key function of sleep. Physiological Genomics *31*, 441–457.

827 Maluck, E., Busack, I., Besseling, J., Masurat, F., Turek, M., Busch, K.E., and
828 Bringmann, H. (2020). A wake-active locomotion circuit depolarizes a sleep-active
829 neuron to switch on sleep. PLoS Biol *18*.

830 Matsuura, T., Suzuki, S., Musashino, A., Kanno, R., and Ichinose, M. (2009). Retention
831 time of attenuated response to diacetyl after pre-exposure to diacetyl in Caenorhabditis
832 elegans. Journal of Experimental Zoology Part A: Ecological Genetics and Physiology
833 *311A*, 483–495.

834 McCloskey, R.J., Fouad, A.D., Churgin, M.A., and Fang-Yen, C. (2017). Food
835 responsiveness regulates episodic behavioral states in Caenorhabditis elegans. J.
836 Neurophysiol. *117*, 1911–1934.

837 Nagy, S., Tramm, N., Sanders, J., Iwanir, S., Shirley, I.A., Levine, E., and Biron, D.
838 (2014a). Homeostasis in C. elegans sleep is characterized by two behaviorally and
839 genetically distinct mechanisms. ELife Sciences *3*, e04380.

840 Nagy, S., Raizen, D.M., and Biron, D. (2014b). Measurements of behavioral quiescence
841 in Caenorhabditis elegans. Methods *68*, 500–507.

842 Newman, A.B., Spiekerman, C.F., Enright, P., Lefkowitz, D., Manolio, T., Reynolds,
843 C.F., and Robbins, J. (2000). Daytime sleepiness predicts mortality and cardiovascular
844 disease in older adults. The Cardiovascular Health Study Research Group. J Am Geriatr
845 Soc *48*, 115–123.

846 Nichols, A.L.A., Eichler, T., Latham, R., and Zimmer, M. (2017). A global brain state
847 underlies C. elegans sleep behavior. Science *356*, eaam6851.

848 Panda, S., Hogenesch, J.B., and Kay, S.A. (2002). Circadian rhythms from flies to
849 human. Nature *417*, 329.

850 Piggott, B.J., Liu, J., Feng, Z., Wescott, S.A., and Xu, X.Z.S. (2011). The Neural Circuits
851 and Synaptic Mechanisms Underlying Motor Initiation in C. elegans. Cell *147*, 922–933.

852 Pujol, N., Torregrossa, P., Ewbank, J.J., and Brunet, J.F. (2000). The homeodomain
853 protein CePHOX2/CEH-17 controls antero-posterior axonal growth in C. elegans.
854 Development *127*, 3361–3371.

855 Raizen, D.M., Zimmerman, J.E., Maycock, M.H., Ta, U.D., You, Y., Sundaram, M.V.,
856 and Pack, A.I. (2008). Lethargus is a Caenorhabditis elegans sleep-like state. Nature
857 *451*, 569–572.

858 Rajaratnam, S.M.W., Howard, M.E., and Grunstein, R.R. (2013). Sleep loss and
859 circadian disruption in shift work: health burden and management. Med. J. Aust. *199*,
860 S11-15.

861 Reppert, S.M., and Weaver, D.R. (2002). Coordination of circadian timing in mammals.
862 Nature *418*, 935.

Sanfilippo-Cohn, B., Lai, S., Zhan, G., Fenik, P., Pratico, D., Mazza, E., and Veasey, S.C. (2006). Sex differences in susceptibility to oxidative injury and sleepiness from intermittent hypoxia. Sleep *29*, 152–159.

Saper, C.B., Scammell, T.E., and Lu, J. (2005). Hypothalamic regulation of sleep and circadian rhythms. Nature *437*, 1257.

Schmidt, M.H. (2014). The energy allocation function of sleep: A unifying theory of sleep, torpor, and continuous wakefulness. Neuroscience & Biobehavioral Reviews *47*, 122–153.

Schwarz, J., Spies, J.-P., and Bringmann, H. (2012). Reduced muscle contraction and a relaxed posture during sleep-like Lethargus. Worm *1*, 12–14.

Sehgal, A., and Mignot, E. (2011). Genetics of Sleep and Sleep disorders. Cell *146*, 194–207.

Siegel, J.M. (2004). The Neurotransmitters of Sleep. J Clin Psychiatry *65*, 4–7.

Singh, K., Chao, M.Y., Somers, G.A., Komatsu, H., Corkins, M.E., Larkins-Ford, J., Tucey, T., Dionne, H.M., Walsh, M.B., Beaumont, E.K., et al. (2011). C. elegans Notch Signaling Regulates Adult Chemosensory Response and Larval Molting Quiescence. Current Biology *21*, 825–834.

Singh, K., Huang, H., and Hart, A.C. (2013). Do C. elegans Sleep? A Closer Look. Sleep *36*, 307–308.

Skora, S., Mende, F., and Zimmer, M. (2018). Energy Scarcity Promotes a Brain-wide Sleep State Modulated by Insulin Signaling in C. elegans. Cell Rep *22*, 953–966.

Spies, J., and Bringmann, H. (2018). Automated detection and manipulation of sleep in C. elegans reveals depolarization of a sleep-active neuron during mechanical stimulation-induced sleep deprivation. Scientific Reports *8*, 9732.

Steuer Costa, W., Van der Auwera, P., Glock, C., Liewald, J.F., Bach, M., Schüler, C., Wabnig, S., Oranth, A., Masurat, F., Bringmann, H., et al. (2019). A GABAergic and peptidergic sleep neuron as a locomotion stop neuron with compartmentalized Ca2+ dynamics. Nat Commun *10*, 4095.

Suda, H., Shouyama, T., Yasuda, K., and Ishii, N. (2005). Direct measurement of oxygen consumption rate on the nematode Caenorhabditis elegans by using an optical technique. Biochemical and Biophysical Research Communications *330*, 839–843.

Tian, L., Hires, S.A., Mao, T., Huber, D., Chiappe, M.E., Chalasani, S.H., Petreanu, L., Akerboom, J., McKinney, S.A., Schreiter, E.R., et al. (2009). Imaging neural activity in worms, flies and mice with improved GCaMP calcium indicators. Nature Methods *6*, 875–881.

Tramm, N., Oppenheimer, N., Nagy, S., Efrati, E., and Biron, D. (2014). Why Do Sleeping Nematodes Adopt a Hockey-Stick-Like Posture? PLoS ONE *9*, e101162.

900 Trojanowski, N.F., Nelson, M.D., Flavell, S.W., Fang-Yen, C., and Raizen, D.M. (2015).
901 Distinct Mechanisms Underlie Quiescence during Two Caenorhabditis elegans Sleep-
902 Like States. J. Neurosci. *35*, 14571–14584.

903 Tsunematsu, T., Kilduff, T.S., Boyden, E.S., Takahashi, S., Tominaga, M., and
904 Yamanaka, A. (2011). Acute Optogenetic Silencing of Orexin/Hypocretin Neurons
905 Induces Slow-Wave Sleep in Mice. J. Neurosci. *31*, 10529–10539.

906 Turek, M., Lewandrowski, I., and Bringmann, H. (2013). An AP2 transcription factor is
907 required for a sleep-active neuron to induce sleep-like quiescence in C. elegans. Curr.
908 Biol. *23*, 2215–2223.

909 Turek, M., Besseling, J., and Bringmann, H. (2015). Agarose Microchambers for Long-
910 term Calcium Imaging of Caenorhabditis elegans. J Vis Exp.

911 Turek, M., Besseling, J., Spies, J.-P., König, S., and Bringmann, H. (2016). Sleep-active
912 neuron specification and sleep induction require FLP-11 neuropeptides to systemically
913 induce sleep. ELife *5*, e12499.

914 Velluti, R. (1997). Interactions between sleep and sensory physiology. Journal of Sleep
915 Research *6*, 61–77.

916 Weber, F., Chung, S., Beier, K.T., Xu, M., Luo, L., and Dan, Y. (2015). Control of REM
917 sleep by ventral medulla GABAergic neurons. Nature *526*, 435–438.

918 Yamuy, J., Fung, S.J., Xi, M., Morales, F.R., and Chase, M.H. (1999). Hypoglossal
919 motoneurons are postsynaptically inhibited during carbachol-induced rapid eye
920 movement sleep. Neuroscience *94*, 11–15.

921 You, Y., Kim, J., Raizen, D.M., and Avery, L. (2008). Insulin, cGMP, and TGF-β Signals
922 Regulate Food Intake and Quiescence in C. elegans: A Model for Satiety. Cell
923 Metabolism *7*, 249–257.

924 Zheng, Y., Brockie, P.J., Mellem, J.E., Madsen, D.M., and Maricq, A.V. (1999).
925 Neuronal Control of Locomotion in C. elegans Is Modified by a Dominant Mutation in the
926 GLR-1 Ionotropic Glutamate Receptor. Neuron *24*, 347–361.

927

928

929 **Figure Legends:**

930

931 **Figure 1. Young adult sleep in wild-type *C. elegans* in "Population behavior"**
932 **microfluidic devices.** (**a**) Schematic of the "Population behavior" microfluidic device,
933 including multiple inlets to switch fluids, four worm entry ports to introduce separate
934 worm populations, and a flow outlet. (**b**) Image frame of a device containing ~100
935 animals, ~25 in each of four separated 16 mm x 15 mm arenas. (**c**) Awake animals
936 roam freely between 200 µm diameter microposts. An awake animal exhibits active
937 contact (filled arrows) around posts along the entire body length. (**d**) Distribution of
938 behavior probability and average speed in the 60 s before and after sleep bouts of at
939 least 1 min. Data are from 4359 sleep bouts from 697 wild-type animals over 12 h that
940 had adjacent wake states at least 1 min (32% of total). Error bar shading in average
941 speed plots indicate 95% confidence interval, and "Forward only" speed excludes
942 pauses and reverse behaviors. Example of 10 individual events are shown. Accuracy of
943 automated sleep bout prediction is assessed in **Table 2**. (**e**) A sleeping animal in the
944 microfluidic device exhibits a straight head posture and the relaxed, bent body passively
945 contacts only 1 – 2 posts (filled arrow) due to fluid flow, leaving others untouched (open
946 arrows). (**f**) Montage (10 s interval) of an animal transitioning between forward motion
947 (red), pausing/creeping motion (pink) and sleep with characteristic head relaxation
948 (blue). Black triangles represent a fixed position for each image located at the final
949 position of the mouth, and microposts were background subtracted for clarity.

950

951 **Figure 2. Dynamics of young adult sleep behavior in the microfluidic**
952 **environment.** (**a**) Raster plot of sleep events (black) over 12 h, sorted by total sleep
953 fraction (n = 535 animals). (**b**) Hourly sleep fraction for all animals from **a** and grouped

into four quartiles by their total 12 h sleep fraction (quartile 1 = most sleep). (**c**) Median sleep fraction, sleep bout duration, and awake bout duration from data in **a**, separated by total sleep quartiles. Error bars indicate 95% confidence interval. (**d**) Changes to sleep behavior over 12 h represented by sleep and awake bout duration. Solid lines represent median durations. Shaded regions represent 25% to 75% quartile durations and dashed lines represent 10% and 90% decile durations of each respective state. (**e**) Average sleep entry and exit transition rate for each hour of experimentation from data in **a**. Separating these curves by total sleep quartile demonstrates consistent sleep exit rates (**f**) but large variation in sleep entry rates (**g**) across wild-type animals.

Figure 3. Effects of fluid flow and sleep perturbation. (**a**) Effect of stationary fluid on sleep behavior over 12 h (*n* = 91 animals). Raster plot of sleep events shown above, and mean hourly sleep fraction below. (**b**) Effect of pulsed buffer flow on sleep behavior over 12 h (*n* = 97 animals). Fluid flow alternated between no flow and moderate flow (0.5 mm/s) every 2 h. Raster plot of sleep events shown above, and mean hourly sleep fraction below. (**c**) Increased sleep during 6 hours of static flow suppressed sleep in 6 subsequent hours of buffer flow (blue) compared with continuous flow controls (black). Plot inset compares average hourly difference in sleep fraction between the variable flow group and constant flow control in hours 2 – 6 (flow effect) and in hours 6 – 12 (sleep compensation effect). (**d**) Decreased sleep during 6 hours of 1.1μM diacetyl stimulation increased sleep in 6 subsequent hours of buffer flow (yellow) compared with buffer controls (black). Plot inset compares average hourly difference in sleep fraction as in c, inset. Statistics were performed using one-way ANOVA with Bonferroni's correction for multiple comparisons; * $P<0.05$; ** $P<0.0001$.

Figure 4. Oxygen and feeding state impact adult sleep in the microfluidic environment. (**a**) Effect of hypoxia on sleep dynamics (*n* = 80–114 animals). Within each group, animals (raster plot rows) are sorted by total sleep fraction. (**b**) Total sleep fraction over 12 h assessing effect of hypoxia on sleep behavior from **a** with bars representing population mean ± s.e.m. and points indicating individual animals. Inset shows median sleep and awake bout duration in low and high oxygen. (**c**) Hourly sleep fraction from data in **a**. (**d**) Effect of feeding and food-related signals comparing sleep behavior in S. Basal buffer, in bacterial food (NA22 *E. coli*, OD600 = 0.35), serotonin 10 µM to mimic feeding response, and a food odor diacetyl 1.1 µM (*n* = 90–123 animals). (**e**) Total sleep fraction over 12 h assessing feeding effect on sleep behavior, as in panel **b**. (**f**) Hourly sleep fraction from data in **d**. (**g**) Hourly sleep fraction for wild-type animals pre-starved for 0–8 h on agar dishes prior to loading in the microfluidic device. (**h**) Total sleep fraction over assessing effect of starvation on sleep behavior from **g** with bars representing population mean ± s.e.m. and points indicating individual animals. Statistics for all plots were performed using one-way ANOVA with Bonferroni's correction for multiple comparisons. For 12 h total sleep fraction plots and median bout duration plots (**b** & **e**): ** P<0.0001; * P<0.05. For hourly sleep fraction (**c** & **f**), significance is noted as * P<0.0001 for the indicated hour.

Figure 5. Effect of genetic perturbations on adult sleep. (**a**) Sleep behavior assessed in 1.1 µM diacetyl (*n* = 45–58 animals) in wild-type and sensory mutants affecting diacetyl odor detection (*odr-10*), general sensation (*tax-4*), and light touch (*mec-4*). Within each group, animals (raster plot rows) are sorted by total sleep fraction. (**b**) Total sleep fraction over 12 h assessing effect of sensory mutations on sleep behavior from **a** with bars representing population mean ± s.e.m. and points indicating

individual animals. (**c**) Hourly sleep fraction from data in **a**. Extended Data Figure 5-1 compares *odr-10* mutant sleep behavior in diacetyl 1.1µM with wild-type animals in S. Basal buffer. (**d**) *ceh-17* mutants deficient in stress-induced sleep exhibit elevated, not reduced, adult sleep behavior in the microfluidic format (*n* = 48 animals). (**e**) Total sleep fraction over 12 h assessing effect of *ceh-17* mutation on sleep, as in panel **b**. (**f**) Hourly sleep fraction from data in **d**. Statistics for all plots were performed using one-way ANOVA with Bonferroni's correction for multiple comparisons. For 12 h total sleep fraction plots (**b** & **e**): ** P<0.0001; * P<0.05. For hourly sleep fraction (**c** & **f**), significance is noted as * P<0.0001 for the indicated hour.

Figure 6. Measuring sleep in "Neural imaging" microfluidic devices. (**a**) Design of microfluidic device for closed-loop sleep assessment, chemical stimulation, and neural imaging. Device contains a single 3 mm x 3 mm arena. (**b**) Sleep is detected in individual animals using pulsed brightfield illumination (λ = 520–550 nm). An awake animal is shown. (**c**) Wild-type adult sleep fraction in "Neural imaging" device (*n* = 7 animals) is similar to the larger "Population behavior" device (*n* = ~100 animals). (**d**) Examples of the frame subtraction method for sleep detection showing awake and sleep cases. Movement Index (M.I.) represents the fraction of body pixels moved between 10 s frame intervals. (**e**) Schematic of sleep decision processing in a single wild-type animal over 12 h in S. Basal: 1. Movement Index with red dotted line representing threshold of M.I. 0.125; 2. Result of threshold M.I. < 0.125; 3. Temporal filtering for 5 consistent state intervals (40 s total); 4. Human ground-truth observation. Accuracy of automated sleep bout prediction over 12 h is assessed in Table 3.

Figure 7. Arousal threshold measurements and sleep-associated neural activity. (**a**) Heatmap showing movement of AIB neuron per frame (0.1 s interval) across 22 pulsed stimulation trials (rows). Animals were stimulated with 1 mM $CuCl_2$ from 5–15 s during each 30 s trial (gray bar). Data sorted by average movement 5 s prior to stimulus, indicating the sleep/awake state for each recording. Repeatable microfluidic stimulus onset and removal within <0.5 s is shown in Extended Data Figure 7-1. (**b**) Average movement pre-stimulus (0–5 s) grouped by sleep state (*n* = 13 Sleep, *n* = 9 Awake). (**c**) Average time to a reversal or avoidance behavior response for sleeping and awake animals. Statistics for **b** and **c** performed using an unpaired two-tailed t-test; ** P<0.001; * P<0.05. (**d**) Image of an animal expressing GCaMP in the RIS neuron. (**e**) Average RIS neuron fluorescence (*n* = 13 sleep events from a single animal) and average neuron centroid movement per frame (0.5 s interval). Neural activity is normalized to minimum and maximum intensity of each RIS neuron trace during the 30 s before and after the awake to sleep transition. Heatmap of all neural recordings is shown below.

Figure 8. Closed-loop stimulation and neural recording in individual free-behaving animals. (**a**) Schematic of closed-loop neural recording set-up for sleep/awake response tracking. Video recording, valve control, and LED triggering were controlled through an Arduino microcontroller. Brightfield images were used to track sleep behavior and fluorescent images were used measure GCaMP calcium transients. Image capture, sleep/awake determination, and chemical stimulation were controlled by computer in a closed loop without user intervention. (**b**) Decision process schematic of closed-loop experiment. Green (brightfield) and blue (fluorescent) shading of decision nodes indicate corresponding illumination source during frame capture. (**c**) Brightfield (λ

= 520–550 nm) and fluorescent (λ = 450–490 nm) images of a freely-moving animal expressing GCaMP in ASH neurons. (**d**) Example showing behavior and neural recording trials in a typical 10 h closed-loop experiment. Behavior patterns and distribution prior to sleep/wake transitions are shown in Extended Data Figure 8-1. (**e**) Peak ASH neural dF/F_0 responses to 1 mM $CuCl_2$ pulses plotted did not show significant adaptation over 10 h. (**f**) Average ASH neural responses in Sleep and Awake states to 10 s aversive $CuCl_2$ pulses (*n* = 18 Sleep, 17 Awake). Neural network map downstream of ASH neurons is plotted in Extended Data Figure 8-2. (**g**) Heatmap of individual ASH responses from **f**. (**h**) Average AIB neural responses in Sleep/Awake states to 10 s $CuCl_2$ pulses (*n* = 13 Sleep, 8 Awake). Extended Data 8-3 shows AIB neural responses aligned to reversal behavior. (**i**) Heatmap of individual AIB responses from **h**. (**j**) Average AVA neural responses in Sleep/Awake states to 10 s $CuCl_2$ pulses (*n* = 13 Sleep, 12 Awake). (**k**) Heatmap of individual AVA responses from **j**.

Figure 9. Appetitive sensory neurons show prolonged neural response during sleep. (**a**) Heatmap showing movement of AWA neuron per frame (0.1 s interval) across 26 pulsed stimulation trials (rows) from two animals in separate experiments. Animals were stimulated with 1.1 μM diacetyl between 5–15 s during each 30 s trial (gray bar). Data are sorted by average movement 5 s prior to stimulus, indicating the sleep/awake state for each recording. (**b**) Heatmap of individual dF/F_0 AWA responses from **a**. (**c**) Time to first movement in sleeping animals (quantified by time of head movement after stimulus onset), compared to initiation of AWA neural activity (*n* = 15 trials). (**d**) Average dF/F_0 AWA neural responses in Sleep/Awake states to 10 s diacetyl pulses from panel **b** (*n* = 15 Sleep, 11 Awake). (**e**) Average dF/F_0 during 15 s after stimulation indicates prolonged neural response in sleep (*n* = 15 trials) versus awake (*n*

= 11 trials) states. (**f**) Peak dF/F_0 in AWA and ASH neurons in response to stimuli during sleep and awake states (*n* = 26-35 trials per condition). Statistics for c, e and f performed using an unpaired two-tailed t-test; ** P<0.001; ns P>0.05.

Table Legends:

Table 1. Detailed statistical analysis. Full statistical information for all main text figures.

Table 2. Population behavior device accuracy assessment. Table of accuracy for automatic sleep tracking in the “Population behavior” device, compared with human ground-truth observation.

Table 3. Neural imaging device accuracy assessment. Table of accuracy for automatic sleep tracking in the “Neural imaging” device, compared with human ground-truth observation.

Extended Data Figures:

Figure 5-1. Hourly sleep fraction comparison between *odr-10* mutants under constant 1.1µM diacetyl exposure to wild-type N2 animals in S. Basal buffer. *odr-10* mutants lack the diacetyl sensory receptor. N2 data from Fig. 2b; *odr-10* data from Fig. 5c.

Figure 7-1. Microfluidic stimulus onset and removal timing measured by flow of fluorescein dye. Fluorescent pixel intensity switches within <0.5 s during a 10 s dye pulse from 5 – 15 s.

Figure 8-1. Pre-stimulus behavior history up to 5 min before 22 stimulation captures during closed-loop stimulation of animals entering and exiting sleep bouts, from Fig. 8d. Average instantaneous sleep fraction is plotted below. Arrowheads represent start of stimulation paradigm in the sleep (blue) or awake (red) state.

Figure 8-2. Neural connections linking copper chloride sensation for reversal behavior upon arousal by stimulus in sleep and wake states in Fig. 8f-k.

Figure 8-3. AIB interneuron activity aligned to point of first reversal response of individual trials, showing AIB rise precedes the delayed reversal in sleeping animals. Data from Fig. 8h,i.

Movies:

Movie 1. Sleep tracking in "Population behavior device". Video shows three portions of a 12 h video tracking sleep behavior in wild-type animals: Early (1.5 h), Middle (5.5 h), and Late (11 h). Animals detected in a sleep state are circled. Video is accelerated 100x.

Movie 2. Example of closed loop system in "Neural imaging device". Video shows an animal expressing GCaMP in the ASH neuron tracked in the closed loop system. First, awake behavior is detected using brightfield illumination and the system applies a stimulus paradigm, 30 s long with a 10-s pulse of 1 μM copper chloride, recording GCaMP fluorescence. Next, a sleep bout is detected and the same stimulus pattern is initiated 1 min after sleep entry. State change detection and stimulus presentation are indicated above. Video is accelerated 37.5x during brightfield behavior and 3x during fluorescent trials.

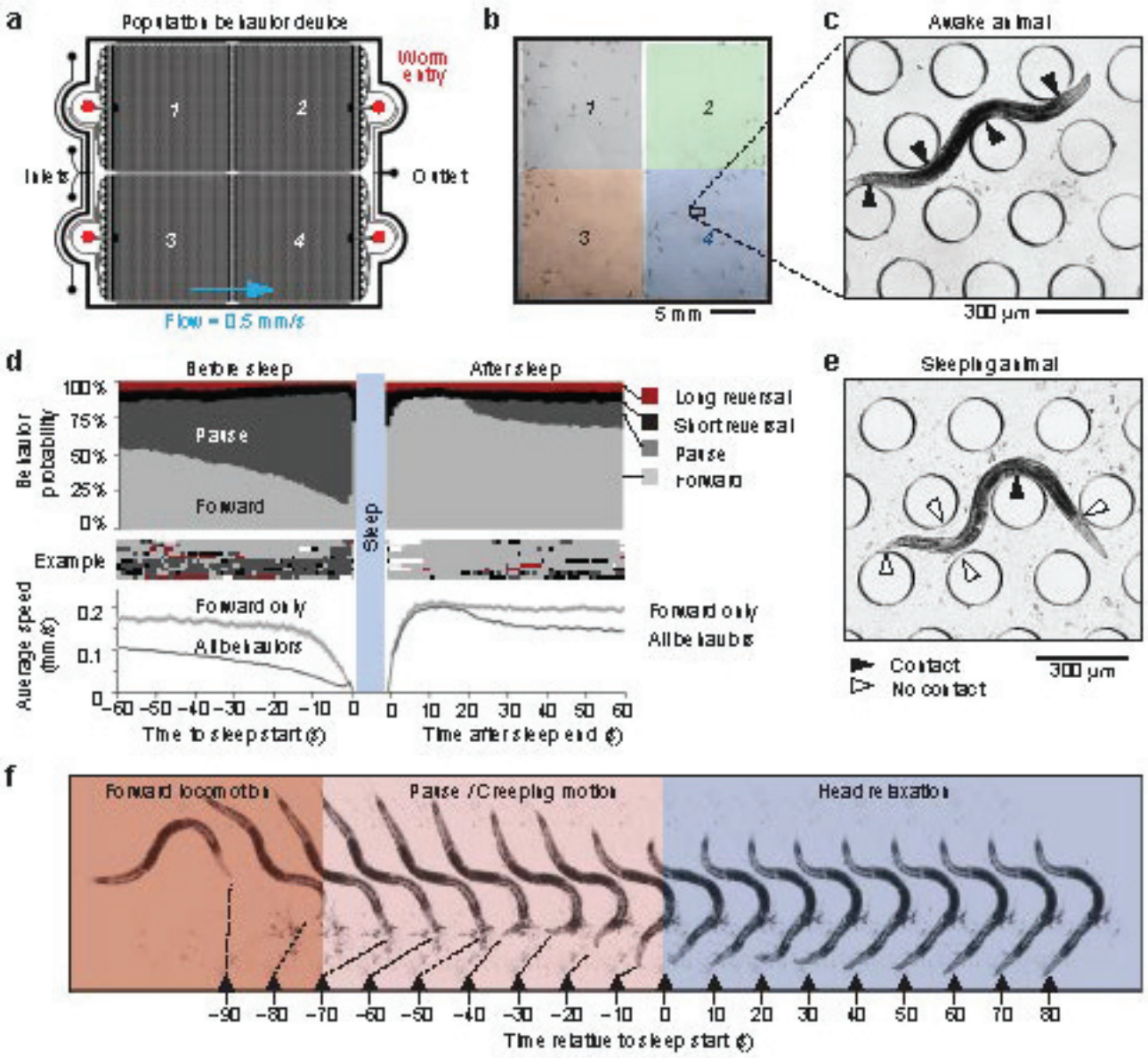

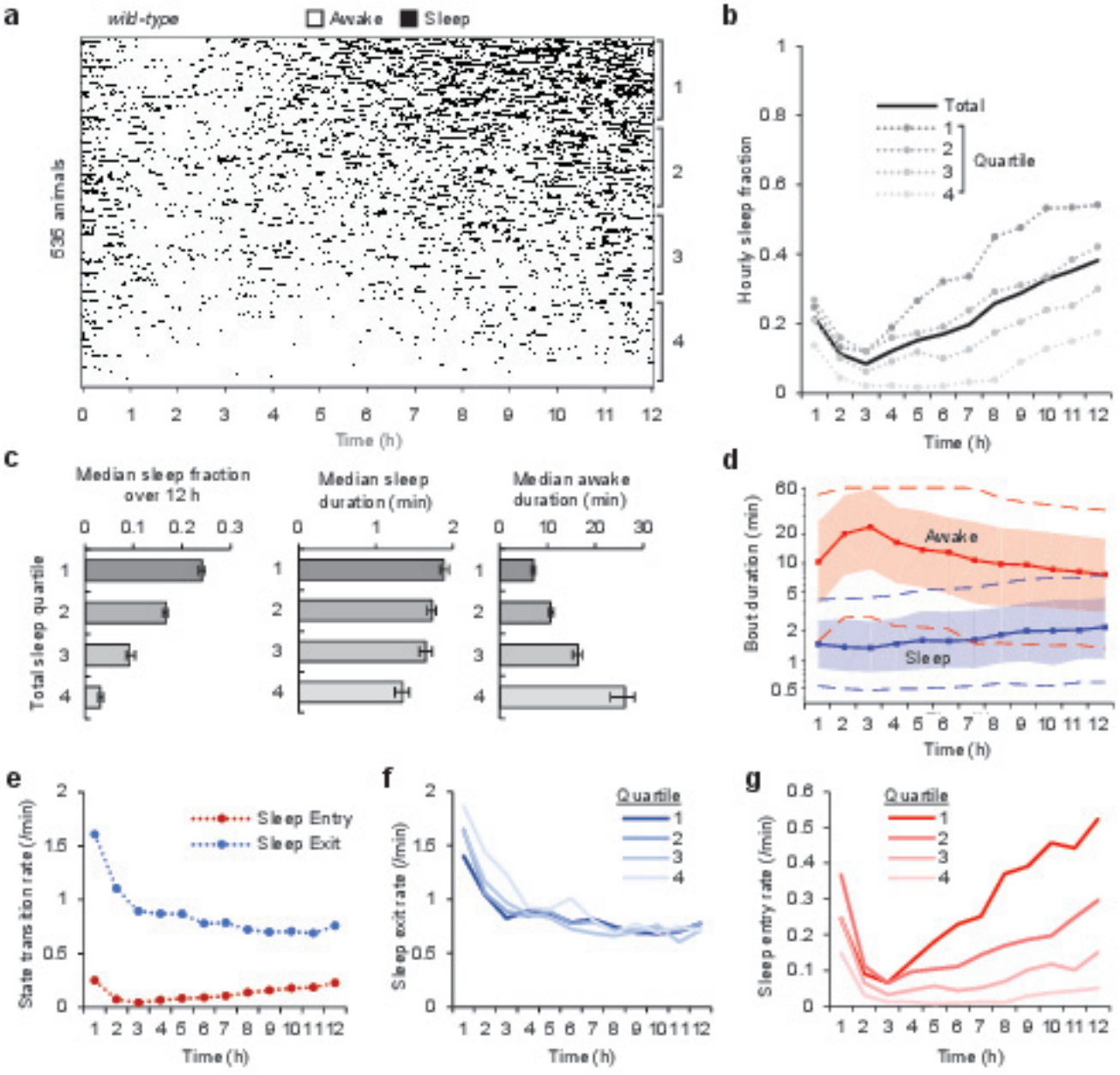

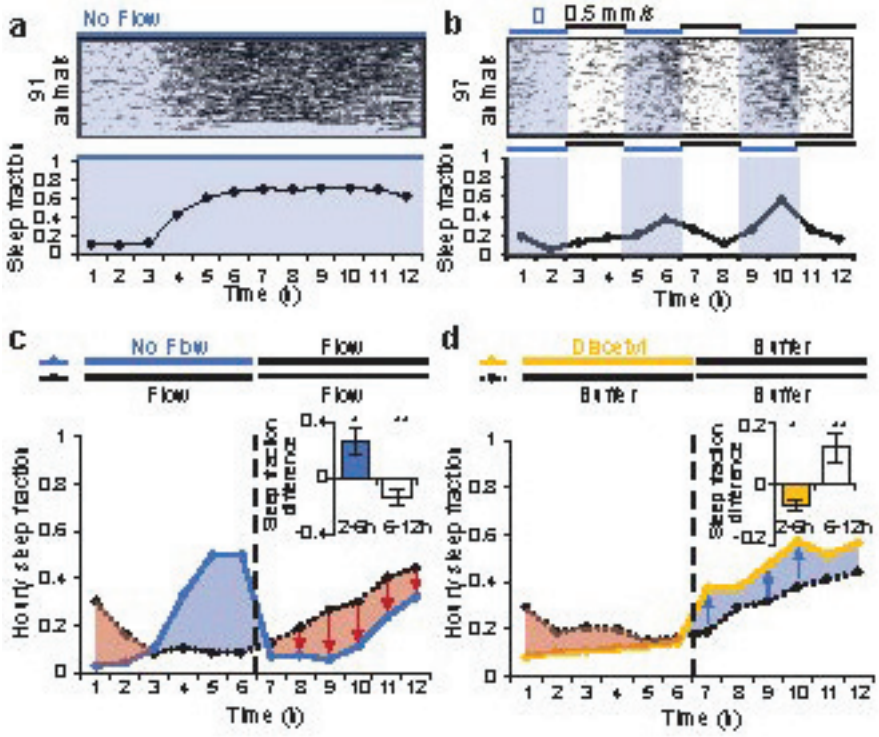

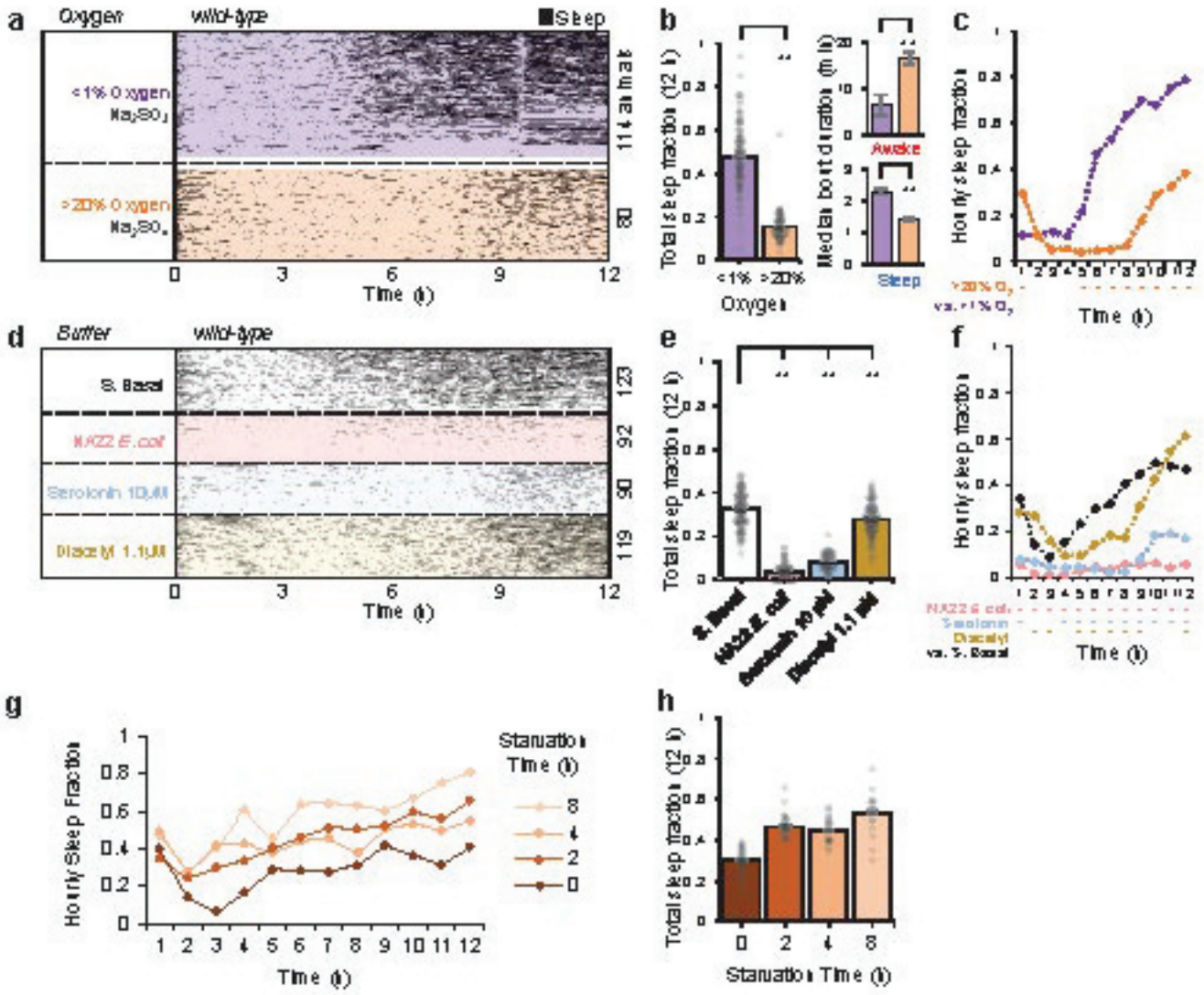

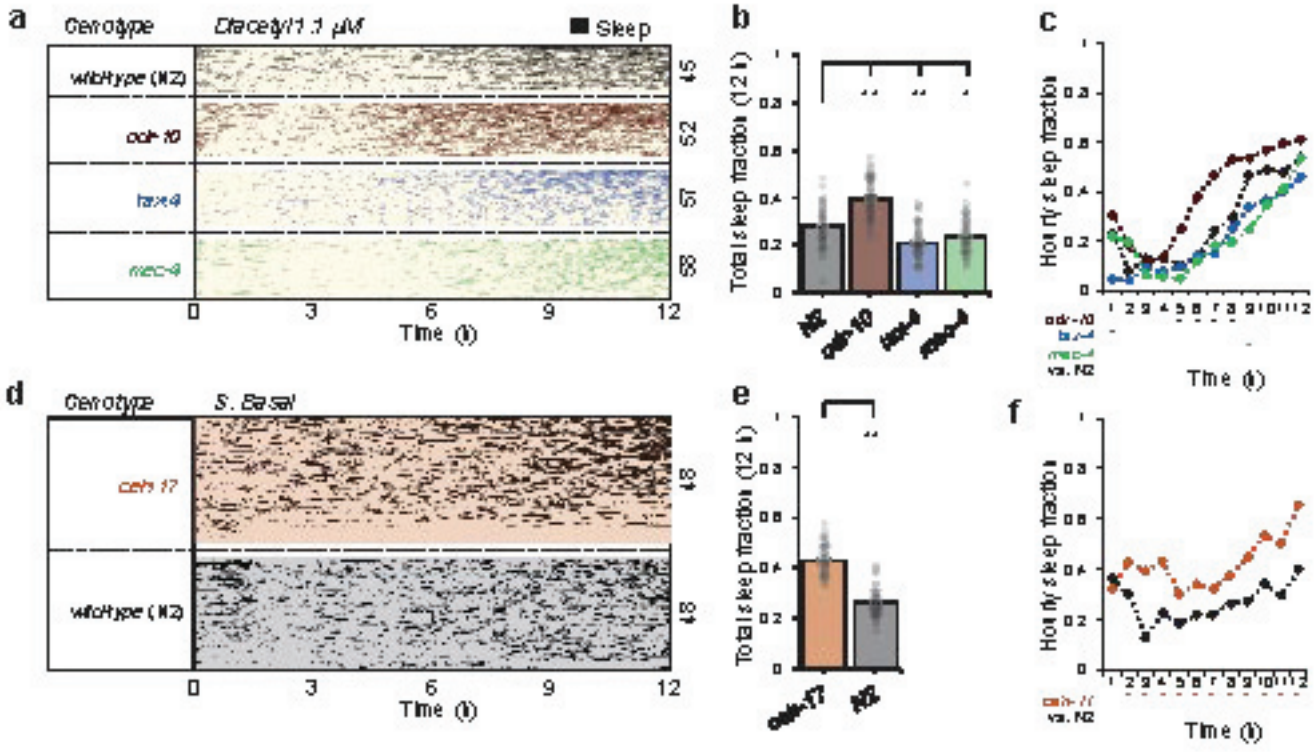

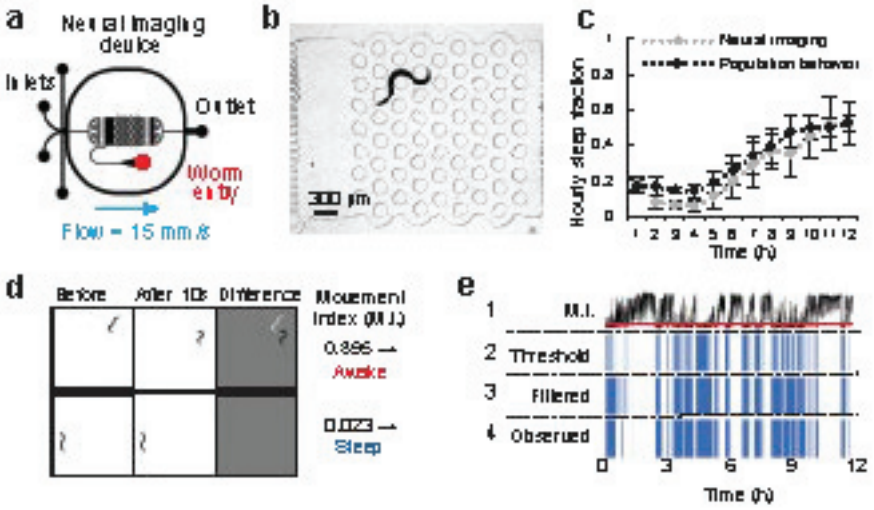

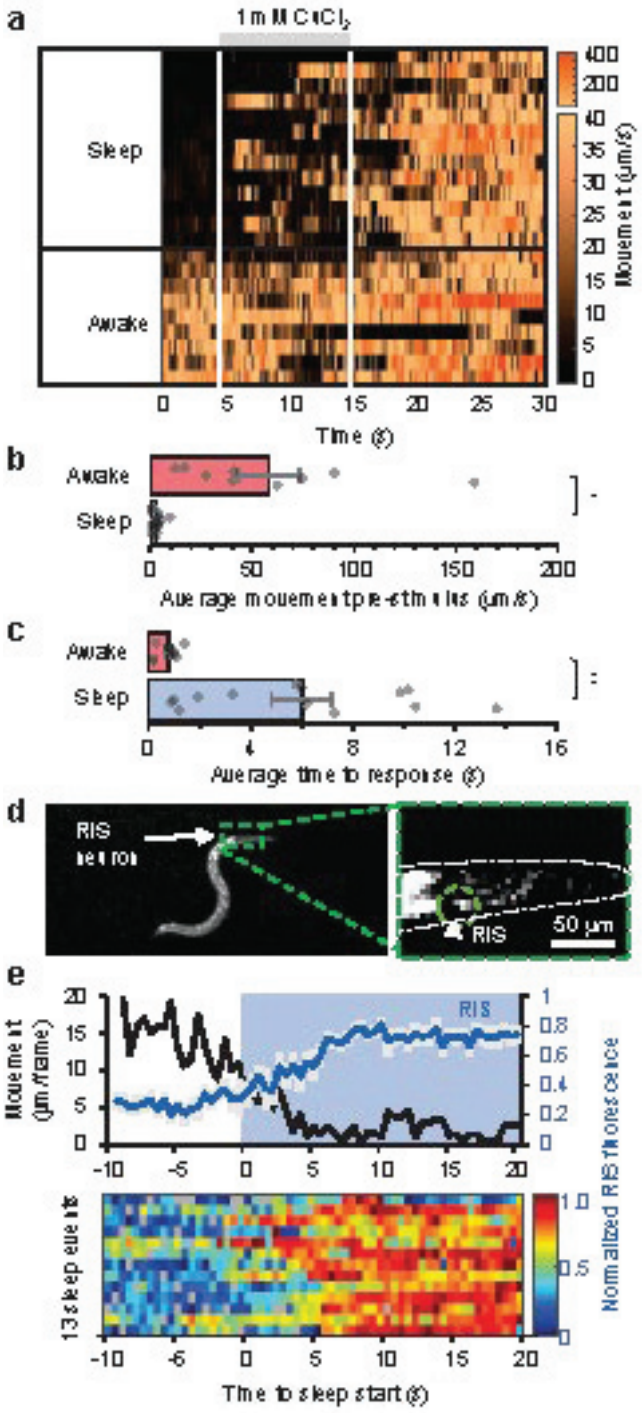

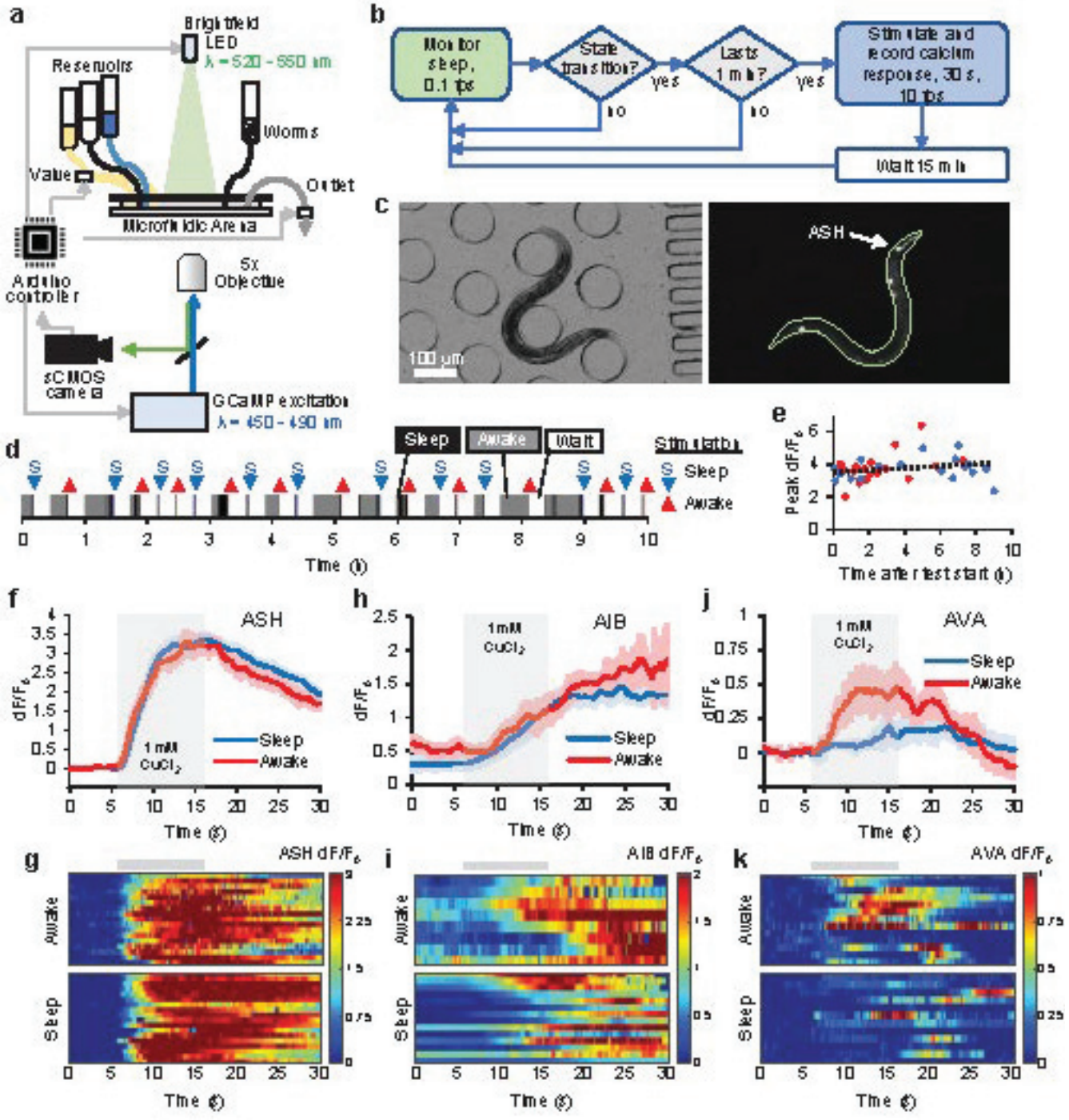

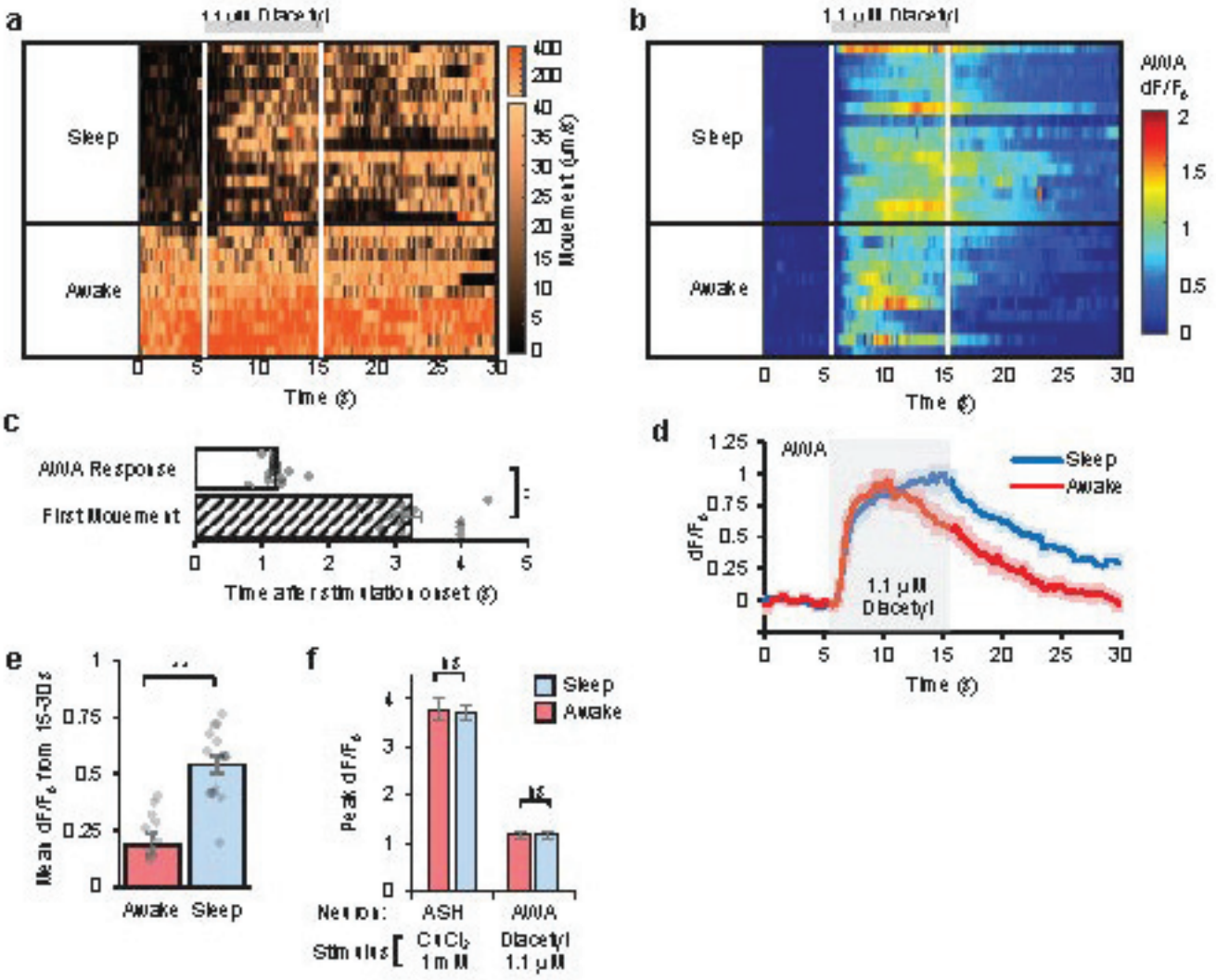

Table 1. Detailed Statistical Analysis.

Figure	Test	*Post hoc* Comparison
3C	Unpaired two-tailed *t*-test	
	Hours 2-6: t = -2.825; df = 6; p = 0.03	
	Hours 6-12: t = 6.371; df = 10; p = 8.13E-05	
3D	Unpaired two-tailed t-test	
	Hours 2-6: t = 2.797; df = 6; p = 0.031	
	Hours 6-12: t = -7.598; df = 10; p = 1.84E-05	
4B	One-way ANOVA	
	Sleep Fraction: $F_{(1,185)}$ = 336.3, p = 1.74E-43	
	Awake Bout Duration: $F_{(1,4228)}$ = 65.4, p = 8.0E-16	
	Sleep Bout Duration: $F_{(1,5802)}$ = 194.1, p = 2.02E-43	
4C	One-way ANOVA	
	Hour 1: $F_{(1,167)}$ = 46.7, p = 1.50E-10	
	Hour 2: $F_{(1,153)}$ = 0.026, p = 0.871	
	Hour 3: $F_{(1,162)}$ = 15.3, p = 1.35E-4	
	Hour 4: $F_{(1,165)}$ = 12.1, p = 6.41E-4	
	Hour 5: $F_{(1,169)}$ = 74.4, p = 4.52E-15	
	Hour 6: $F_{(1,172)}$ = 235.2, p = 5.21E-34	
	Hour 7: $F_{(1,164)}$ = 358.2, p = 4.25E-43	
	Hour 8: $F_{(1,162)}$ = 361.4, p = 4.18E-43	
	Hour 9: $F_{(1,163)}$ = 382.2, p = 1.37E-44	
	Hour 10: $F_{(1,172)}$ = 135.7, p = 1.72E-23	
	Hour 11: $F_{(1,152)}$ = 166.7, p = 3.26E-26	
	Hour 12: $F_{(1,153)}$ = 122.6, p = 2.66E-21	
4E	One-way ANOVA	Bonferroni's correction for multiple comparisons
	S. Basal vs. NA22, Serotonin, and Diacetyl: $F_{(3,417)}$ = 584.8	S. Basal vs. NA22: p = 2.83E-123 S. Basal vs. Serotonin: p = 4.21E-123 S. Basal vs. Diacetyl: p = 3.13E-08
4F	One-way ANOVA	Bonferroni's correction for multiple comparisons
	Hour 1: $F_{(3,368)}$ = 57.9	S. Basal vs. NA22: p = 2.72E-21 S. Basal vs. Serotonin: p = 5.15E-20 S. Basal vs. Diacetyl: p = 0.22
	Hour 2: $F_{(3,369)}$ = 39.5	S. Basal vs. NA22: p = 1.67E-06 S. Basal vs. Serotonin: p = 0.027 S. Basal vs. Diacetyl: p = 3.74E-07
	Hour 3: $F_{(3,394)}$ = 33.6	S. Basal vs. NA22: p = 1.34E-05 S. Basal vs. Serotonin: p = 0.039 S. Basal vs. Diacetyl: p = 5.40E-06
	Hour 4: $F_{(3,393)}$ = 34.5	S. Basal vs. NA22: p = 9.22E-18 S. Basal vs. Serotonin: p = 1.06E-11 S. Basal vs. Diacetyl: p = 0.0012
	Hour 5: $F_{(3,396)}$ = 57.2	S. Basal vs. NA22: p = 1.37E-24 S. Basal vs. Serotonin: p = 1.58E-22 S. Basal vs. Diacetyl: p = 2.04E-14
	Hour 6: $F_{(3,397)}$ = 66.4	S. Basal vs. NA22: p = 2.54E-25 S. Basal vs. Serotonin: p = 8.96E-29 S. Basal vs. Diacetyl: p = 4.40E-13

	Hour 7: $F_{(3,397)} = 104.8$	S. Basal vs. NA22: $p = 8.01E-36$ S. Basal vs. Serotonin: $p = 6.23E-42$ S. Basal vs. Diacetyl: $p = 6.29E-14$
	Hour 8: $F_{(3,395)} = 132.6$	S. Basal vs. NA22: $p = 5.78E-42$ S. Basal vs. Serotonin: $p = 4.70E-51$ S. Basal vs. Diacetyl: $p = 8.84E-26$
	Hour 9: $F_{(3,398)} = 141.3$	S. Basal vs. NA22: $p = 1.15E-48$ S. Basal vs. Serotonin: $p = 6.19E-47$ S. Basal vs. Diacetyl: $p = 1.61E-10$
	Hour 10: $F_{(3,386)} = 109.6$	S. Basal vs. NA22: $p = 2.24E-42$ S. Basal vs. Serotonin: $p = 6.76E-27$ S. Basal vs. Diacetyl: $p = 0.029$
	Hour 11: $F_{(3,387)} = 165.4$	S. Basal vs. NA22: $p = 2.20E-47$ S. Basal vs. Serotonin: $p = 3.00E-26$ S. Basal vs. Diacetyl: $p = 0.061$
	Hour 12: $F_{(3,387)} = 191.8$	S. Basal vs. NA22: $p = 2.50E-39$ S. Basal vs. Serotonin: $p = 6.67E-27$ S. Basal vs. Diacetyl: $p = 1.07E-09$
5B	One-way ANOVA	Bonferroni's correction for multiple comparisons
	N2 vs. *odr-10*, *tax-4*, and *mec-4* : $F_{(3,207)} = 62.5$	N2 vs. *odr-10*: $p = 2.93E-11$ N2 vs. *tax-4*: $p = 2.66E-05$ N2 vs. *mec-4*: $p = 0.026$
5C	One-way ANOVA	Bonferroni's correction for multiple comparisons
	Hour 1: $F_{(3,191)} = 21.0$	N2 vs. *odr-10*: $p = 0.089$ N2 vs. *tax-4*: $p = 6.93E-06$ N2 vs. *mec-4*: $p = 1$
	Hour 2: $F_{(3,188)} = 8.81$	N2 vs. *odr-10*: $p = 0.171$ N2 vs. *tax-4*: $p = 1$ N2 vs. *mec-4*: $p = 0.0076$
	Hour 3: $F_{(3,192)} = 2.87$	N2 vs. *odr-10*: $p = 1$ N2 vs. *tax-4*: $p = 1$ N2 vs. *mec-4*: $p = 0.049$
	Hour 4: $F_{(3,197)} = 6.57$	N2 vs. *odr-10*: $p = 1$ N2 vs. *tax-4*: $p = 0.039$ N2 vs. *mec-4*: $p = 0.0024$
	Hour 5: $F_{(3,196)} = 25.1$	N2 vs. *odr-10*: $p = 2.63E-07$ N2 vs. *tax-4*: $p = 1$ N2 vs. *mec-4*: $p = 0.255$
	Hour 6: $F_{(3,199)} = 34.9$	N2 vs. *odr-10*: $p = 2.36E-12$ N2 vs. *tax-4*: $p = 1$ N2 vs. *mec-4*: $p = 1$
	Hour 7: $F_{(3,201)} = 33.3$	N2 vs. *odr-10*: $p = 6.91E-08$ N2 vs. *tax-4*: $p = 0.078$ N2 vs. *mec-4*: $p = 0.493$
	Hour 8: $F_{(3,201)} = 34.7$	N2 vs. *odr-10*: $p = 7.42E-09$ N2 vs. *tax-4*: $p = 1$ N2 vs. *mec-4*: $p = 0.072$
	Hour 9: $F_{(3,197)} = 21.2$	N2 vs. *odr-10*: $p = 1$ N2 vs. *tax-4*: $p = 0.0053$ N2 vs. *mec-4*: $p = 1.06E-06$
	Hour 10: $F_{(3,192)} = 16.2$	N2 vs. *odr-10*: $p = 0.426$ N2 vs. *tax-4*: $p = 0.0064$ N2 vs. *mec-4*: $p = 8.39E-4$

	Hour 11: $F_{(3,194)}$ = 8.41	N2 vs. *odr-10*: p = 0.294 N2 vs. *tax-4*: p = 0.111 N2 vs. *mec-4*: p = 0.680
	Hour 12: $F_{(3,194)}$ = 3.98	N2 vs. *odr-10*: p = 0.848 N2 vs. *tax-4*: p = 0.500 N2 vs. *mec-4*: p = 1
5E	One-way ANOVA	
	$F_{(1,94)}$ = 180.0, p = 1.47E-23	
5F	One-way ANOVA	
	Hour 1: $F_{(1,88)}$ = 0.032, p = 0.857	
	Hour 2: $F_{(1,86)}$ = 7.36, p = 0.008	
	Hour 3: $F_{(1,84)}$ = 45.4, p = 1.91E-09	
	Hour 4: $F_{(1,90)}$ = 21.6, p = 1.14E-05	
	Hour 5: $F_{(1,90)}$ = 11.7, p = 9.53E-04	
	Hour 6: $F_{(1,89)}$ = 12.4, p = 6.93E-04	
	Hour 7: $F_{(1,88)}$ = 5.53, p = 0.021	
	Hour 8: $F_{(1,92)}$ = 10.1, p = 0.002	
	Hour 9: $F_{(1,92)}$ = 18.8, p = 3.69E-05	
	Hour 10: $F_{(1,87)}$ = 24.4, p = 3.69E-06	
	Hour 11: $F_{(1,88)}$ = 18.9, p = 3.66E-05	
	Hour 12: $F_{(1,85)}$ = 34.5, p = 8.00E-08	
7B	Unpaired two-tailed *t*-test	
	t = 4.343; df = 20; p = 3.16E-04	
7C	Unpaired two-tailed *t*-test	
	t = -3.694; df = 20; p = 0.0014	
8E	Linear Regression	
	Result: Peak dF/F_0 = 3.518+0.065*h	
	S.E.M of slope: 0.049	
	p of slope: 0.193	
9C	Unpaired two-tailed *t*-test	
	t = -13.023; df = 28; p = 2.11E-13	
9E	Unpaired two-tailed *t*-test	
	t = -5.5; df = 24; p = 1.18E-05	
9F	Unpaired two-tailed *t*-test	
	ASH: t = 0.452; df = 33; p = 0.654	
	AWA: t = -0.146; df = 24; p = 0.885	

Table 2. Population behavior device accuracy assessment.

Population behavior device		Observation	
		Sleep	Awake
Prediction	Sleep	255	19
	Awake	5	221
Accuracy		95.2%	
False Discovery Rate		1.9%	
False Omission Rate		7.9%	

Table 3. Neural imaging device accuracy assessment.

Neural imaging device		Observation	
		Sleep	Awake
Prediction	Sleep	1969	144
	Awake	123	1810
Accuracy		93.4%	
False Discovery Rate		5.9%	
False Omission Rate		7.4%	